MLM-2809
UC-4 & UC-22

Mound Facility Activities in Chemical and Physical Research: July-December 1980

Issued: April 10, 1981

MOUND FACILITY
Miamisburg, Ohio 45342

operated by
MONSANTO RESEARCH CORPORATION
a subsidiary of Monsanto Company

for the
U. S. DEPARTMENT OF ENERGY

Contract No. DE-AC04-76-DP00053

Foreword

This report is issued semiannually by Mound Facility. Under the sponsorship of the DOE Division of Basic Energy Sciences, Mound Facility is responsible for research in the physical sciences to further the progress of science and technology in the public interest. This report is submitted by W. T. Cave, Director of Nuclear Operations, and R. E. Vallee, Manager of Technology Applications and Development, from contributions prepared by W. M. Rutherford, Science Fellow (Thermal Diffusion); W. L. Taylor, Science Fellow (Gas Dynamics and Cryogenics); G. L. Silver, Science Fellow (Separation Chemistry); L. J. Wittenberg, Leader, Metal Hydride Research; and from members of the Isotope Separation Section: W. R. Wilkes, Isotope Separation Manager; E. D. Michaels, Leader, Isotope Separation Engineering; and B. E. Jepson, Senior Research Specialist, Metal Isotope Separation Research and Development.

These reports are not intended to constitute publication in any sense of the word. Final results will either be submitted for publication in regular professional journals or be published in the form of MLM topical reports.

Previous reports in this series are:

MLM-2168	MLM-2506
MLM-2198	MLM-2555
MLM-2241	MLM-2590
MLM-2296	MLM-2654
MLM-2354	MLM-2727
MLM-2414	MLM-2756
MLM-2450	

Contents

An experimental liquid thermal diffusion cascade was used to separate 230 g of chlorine-35 enriched to 99.6%. The working fluid for the separation was methyl chloride.

III. Calculations in plutonium chemistry

I. Low temperature research

Thermometry

G. T. McConville

Determination of temperature at low temperatures is accomplished by measuring a resistance that has been compared to a standard that is traceable to the National Bureau of Standards. The standard thermometers are compared at fixed point temperatures. In the temperature range between 10 and 30 Kelvin, the fixed points [1] are at the triple point of H_2, 13.81 K; the normal boiling point of H_2, 20.28 K; the triple point of natural neon, 24.55; and the normal boiling point of neon, 27.01 K. In making vapor pressure measurements on deuterium, one cannot use the H_2 fixed points for reference temperatures because H_2 adsorbed in the system produces excess HD in the D_2 vapor pressure measurements. Thus, in the vapor pressure cryostat there has been uncertainty both about the low temperature and our temperature scale (see MLM-2198). A second problem showed up in the fitting of the neon vapor pressure data which is displayed in Figure I-1.

The fit to the standard vapor pressure equation produced an oscillation as a function of temperature corresponding to $\pm$0.02 K at the low temperature end. An oscillation of this sort usually means the fitting function does not describe the data. There are actually two fitting functions. The vapor pressure equation and the resistance vs. temperature function for the Rosemont Engineering platinum thermometer [2]. A way to test the second function is to use the measured vapor pressure of other workers as the thermometer. Furukawa [3], of NBS, has

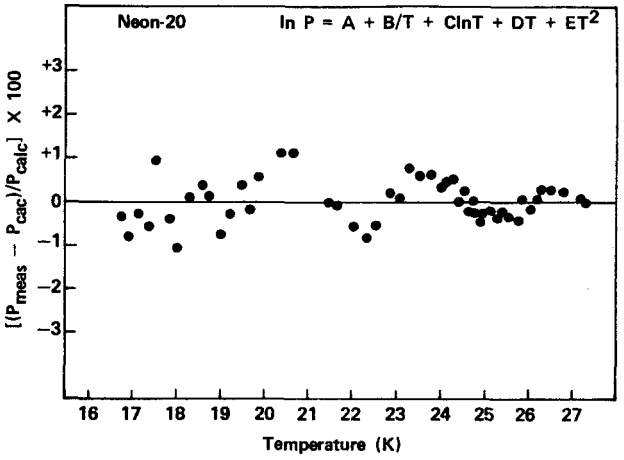

FIGURE I-1 - Oscillation in neon vapor pressure when fitted to standard equation. Temperature determined from Rosemont Engineering calibration.

measured liquid natural Ne, ^{20}Ne and ^{22}Ne. Grilly, of LASL, has measured solid natural Ne [4], and liquid and solid D_2 [5], containing 0.8% HD (research grade chemically pure D_2). We have made a new set of ^{20}Ne measurements and research grade D_2 with 0.84% HD using the new Leeds and Northrup platinum thermometer resistance bridge. Now for a given vapor pressure one can interpret temperature two ways: from the Rosemont calibration or from other vapor pressure data. Figure I-2 shows the comparison for ^{20}Ne using Grilly as the temperature standard. His data only go down to 20 K. The oscillation appears in the relative temperature of the Rosemont calibration.

Now one can make new temperature vs. resistance curves by taking the resistance at a given vapor pressure and the temperature calculated from the vapor pressure curves of Furukawa's or Grilly's measurements. At very low temperatures the relation between resistance and temperature is as that given in Table I-1 where B_n is the best fit from the data. Figure

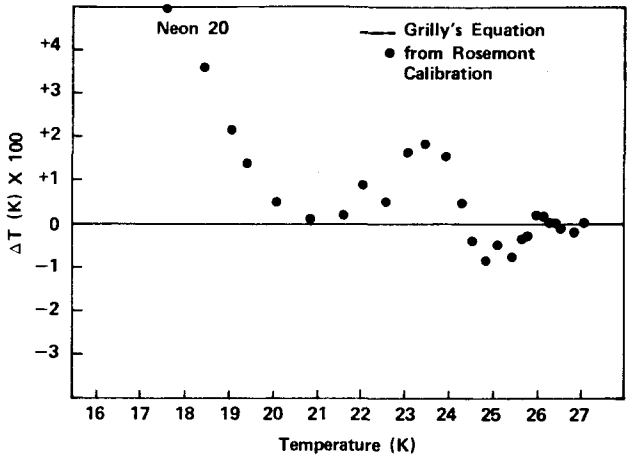

FIGURE I-2 - Comparison of temperatures determined from Grilly's vapor pressure equation and the Rosemont platinum thermometer calibration.

I-3 then shows that the oscillation is missing from the vapor pressure fit using temperature determined in this way. The

Table I-1 - LOW TEMPERATURE VS. RESISTANCE EQUATION

$$R = A + \sum_{n=1}^{5} B_n T^n$$

$$A = R_0 = 0.17371$$

$$B_1 = -0.723619 \times 10^{-2}$$
$$B_2 = 0.259720 \times 10^{-2}$$
$$B_3 = -0.281698 \times 10^{-3}$$
$$B_4 = 0.184811 \times 10^{-4}$$
$$B_5 = -0.250266 \times 10^{-6}$$

Rosemont calibration points also represent a temperature vs. resistance relationship. If one fits them to the equation in Table I-1, the results are shown in Figure I-4. The source of the oscillation in the vapor pressure is clearly in the Rosemont calibration points for the platinum thermometer.

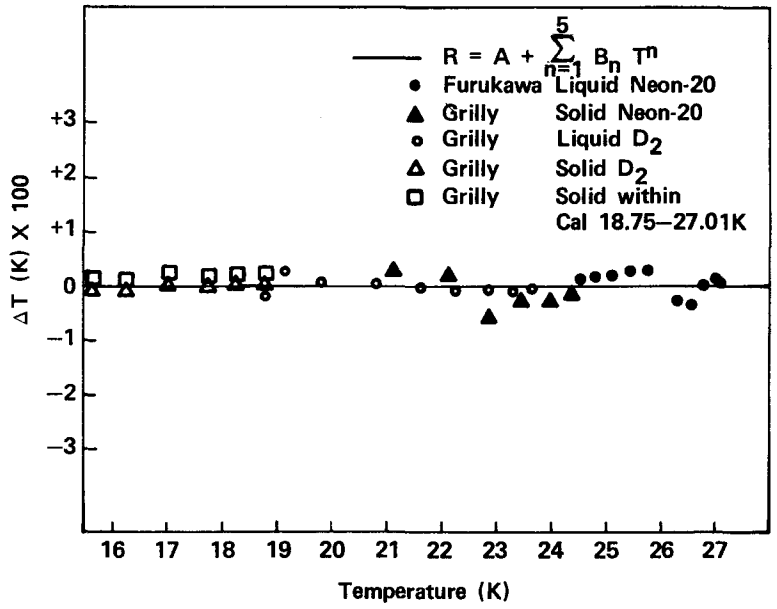

FIGURE I-3 - A fit of temperature from several vapor pressure measurements to measured resistance of the platinum thermometer using a fifth order polynomial in temperature.

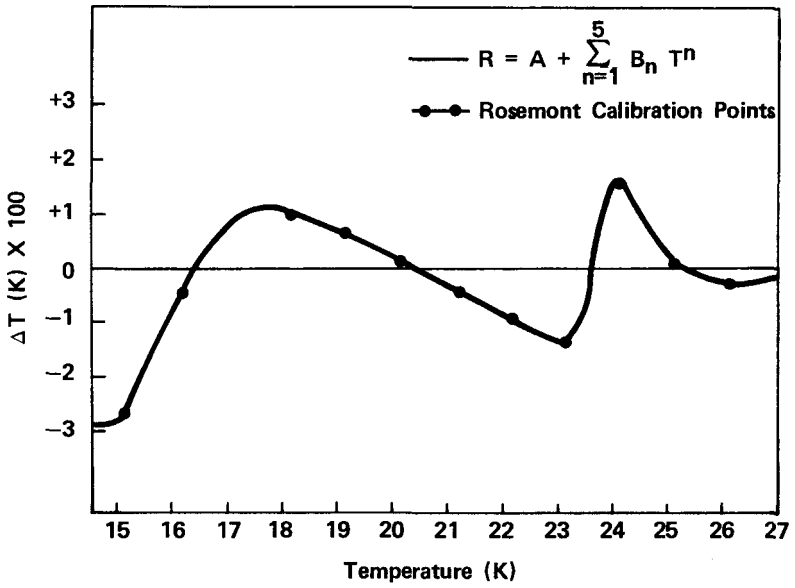

FIGURE I-4 - A fit of the Rosemont calibration temperatures to the same form of equation as in Figure I-3.

Differential vapor pressure measurements

G. T. McConville

Analysis of several differential vapor pressure measurements of ortho-para D_2 mixtures has been completed. It was found that precise knowledge of the HD concentration in the mixtures is necessary to make sense of the experimental results. Three different sets of experimental results are shown in Figure I-5. There are two data sets for normal D_2 (nD_2-para = 33%) measured against equilibrium D_2 (eD_2-para = 2.1%) and one set of data for a 19% para mixture against equilibrium D_2. The different samples had small amounts of HD of the order of 0.1% in them.

The difference in HD concentration is significant because, when the data were first analyzed, the HD concentrations in the 12/13/79 and 12/18/79 runs for the n-D_2 and 19% para were reversed with the e-D_2 samples. Having the concentrations reversed made it look as if J/(X-Xe), where X is the para concentration, was independent of X in the liquid phase. Elimination of this inconsistency produced nearly identical results for the nD_2 vs. eD_2 runs of 12/13/79 and 2/12/80. The quantity J is determined from the experimental quantities in the following expression:

$$J = \frac{\Delta P}{P_e}\left(1 + \frac{BP_e}{kT}\right) + \left(\frac{\Delta P}{P_e}\right)^2 \qquad (1)$$

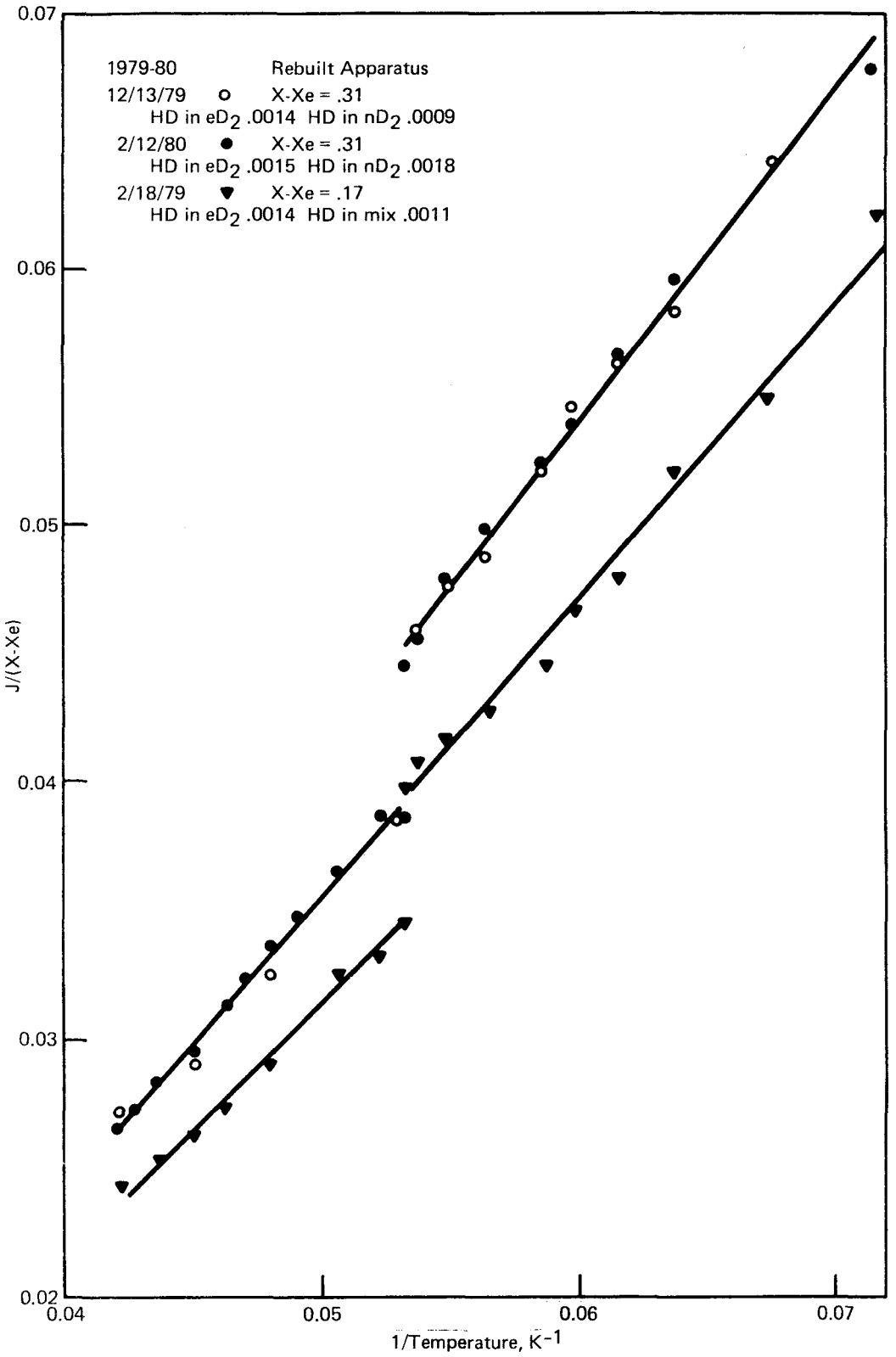

FIGURE I-5 - Differential vapor pressure of two ortho-para mixtures against equilibrium deuterium as a function of reciprocal temperature.

where B is the second virial coefficient, $\Delta P = P_{mix} - P_e$ where P_e is the vapor pressure of the equilibrium D_2. The quantity $J(X-X_e)$ is related to the excess free energy by:

$$RT\frac{J}{X-X_e} = \frac{G-G_e}{X-X_e} + RT \ln \frac{P_2^{o*}}{P_1^{o*}} \qquad (2)$$

where from the analysis of Bellmans and Babyantz [6]:

$$\frac{G^E-Ge^E}{X-X_e} = [1-(X+X_e)]\Lambda[\frac{\theta_r}{T} - \frac{59}{80}] + A_{10} - \frac{A_{11}+A_{00}}{2} \qquad (3)$$

$$RT \ln \frac{P_2^{o*}}{P_1^{o*}} = \Lambda[\frac{\theta_r}{T} - \frac{59}{80} + \frac{25}{48}] + 1/2(A_{11}-A_{00}). \qquad (4)$$

The constant Λ is related to the quadrupole moment Q through the expressions:

$$\frac{\Lambda}{R} = \frac{70}{36} z \frac{\Gamma^2}{K^2\theta_r} \text{ and } \Gamma = \frac{6}{25}\frac{e^2Q^2}{r_o^5} \qquad (5)$$

where z is the number of nearest neighbors and r_o is the nearest neighbor distance in the solid.

One problem with the data in Figure I-2 is that it is not in agreement with the only previous data of Meckstroth and White [7]. Figure I-6 compares present data with $(X-X_e)$ of 0.31 and 0.17 with the closest $(X-X_e)$ data of Meckstroth and White of $(X-X_e)$ of 0.278 and 0.142. There is considerable disagreement. The figure shows a dashed line which represents a nD_2 vs. eD_2 measurement for the liquid only. The experiment was done just after the ΔP pressure transducer was replaced and it was found that there was nearly 1% more HD on the eD_2 side of the system after the measurement than before. It was then decided to see what would happen if one took Meckstroth's $(X-X_e) = 0.278$ data and subtracted values corresponding to the same $(X-X_e)$, assuming a linear variation between the present $(X-X_e) = 0.31$ and 0.17 data. It turns out the difference in ΔP corresponds to a nearly constant percentage of HD $\sim$ 0.6% for the liquid and solid points as shown in Table I-2. It appears that the measurements of Meckstroth may have had an undetected excess of HD in the eD_2 material.

Table I-2 - PERCENTAGE HD TO MAKE DIFFERENCE BETWEEN DATA OF MECKSTROTH AND WHITE AND PRESENT DATA

Liquid		Solid	
T	% HD	T	% HD
22.38	0.60	18.45	0.69
21.57	0.59	17.87	0.60
20.90	0.57	17.13	0.62
20.16	0.55	16.12	0.65
19.45	0.53	15.19	0.69
18.73	0.53		

Returning to the analysis of the data in Figure I-5, if one multiplies J/(X-Xe) by RT, as shown in Figure I-7, one can see a different temperature dependence in the liquid than in the solid. The discontinuity at the triple point [8] is due to the decrease in the number of nearest neighbors in going from the solid to the liquid. Normalizing the liquid data to 12 nearest neighbors by multiplying RTJ/(X-Xe) by 12/z is shown in Figure I-8. It appears that the nonspherical interaction per nearest neighbor is independent of being in the liquid or solid phase.

The difference in the two lines in Figure I-8 is given by:

$$\Delta = RT[\frac{J_1}{X_1-Xe} - \frac{J_2}{X_2-X_e}] = (X_2-X_1)\Lambda[\frac{\theta_r}{T} - \frac{59}{80}]. \qquad (6)$$

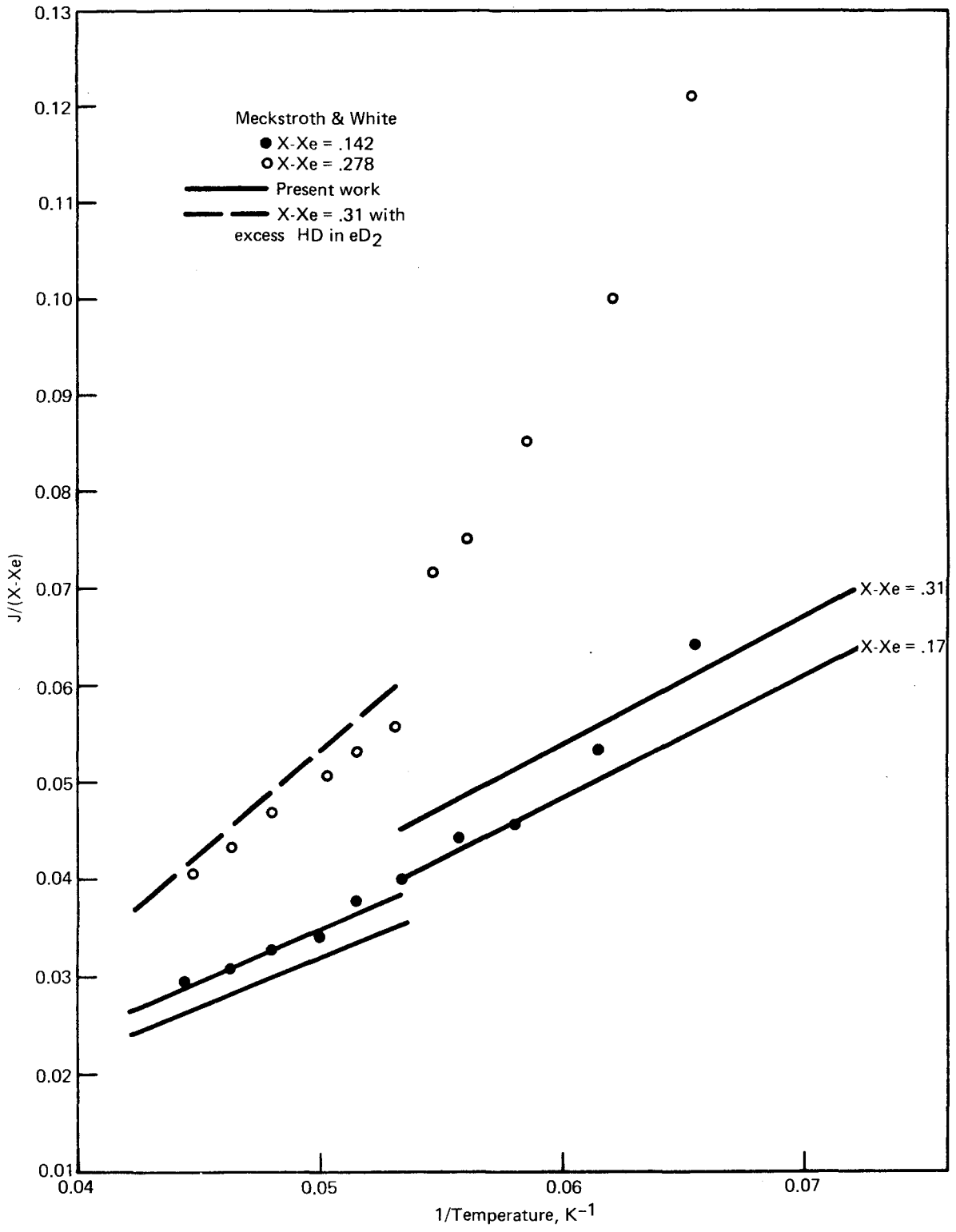

FIGURE I-6 - Comparison of differential vapor pressure data of Meckstroth and White with present data.

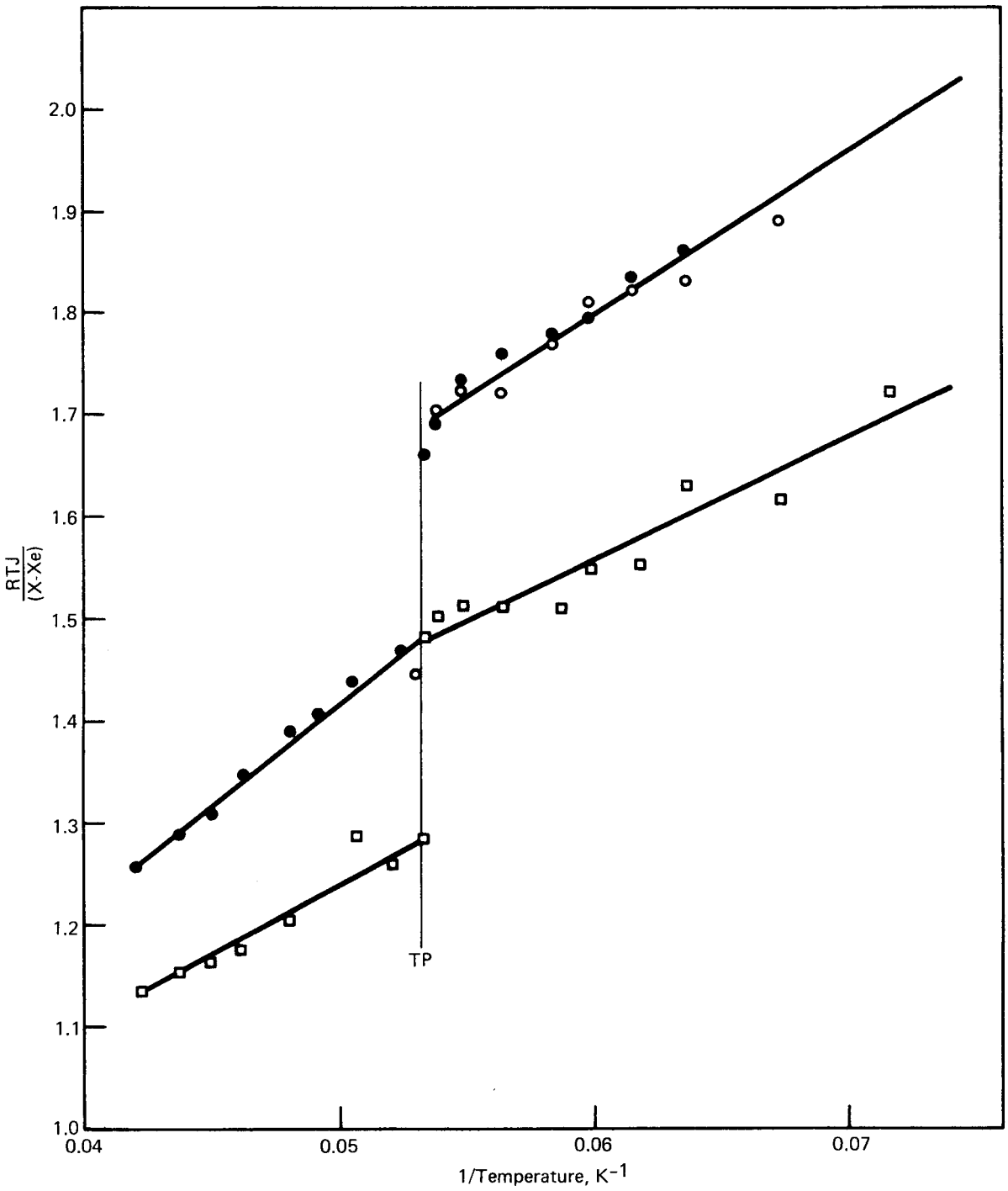

FIGURE I-7 - Data in Figure I-5 multiplied by RT which then are directly proportional to the excess free energy, $G^E-G^E_e$.

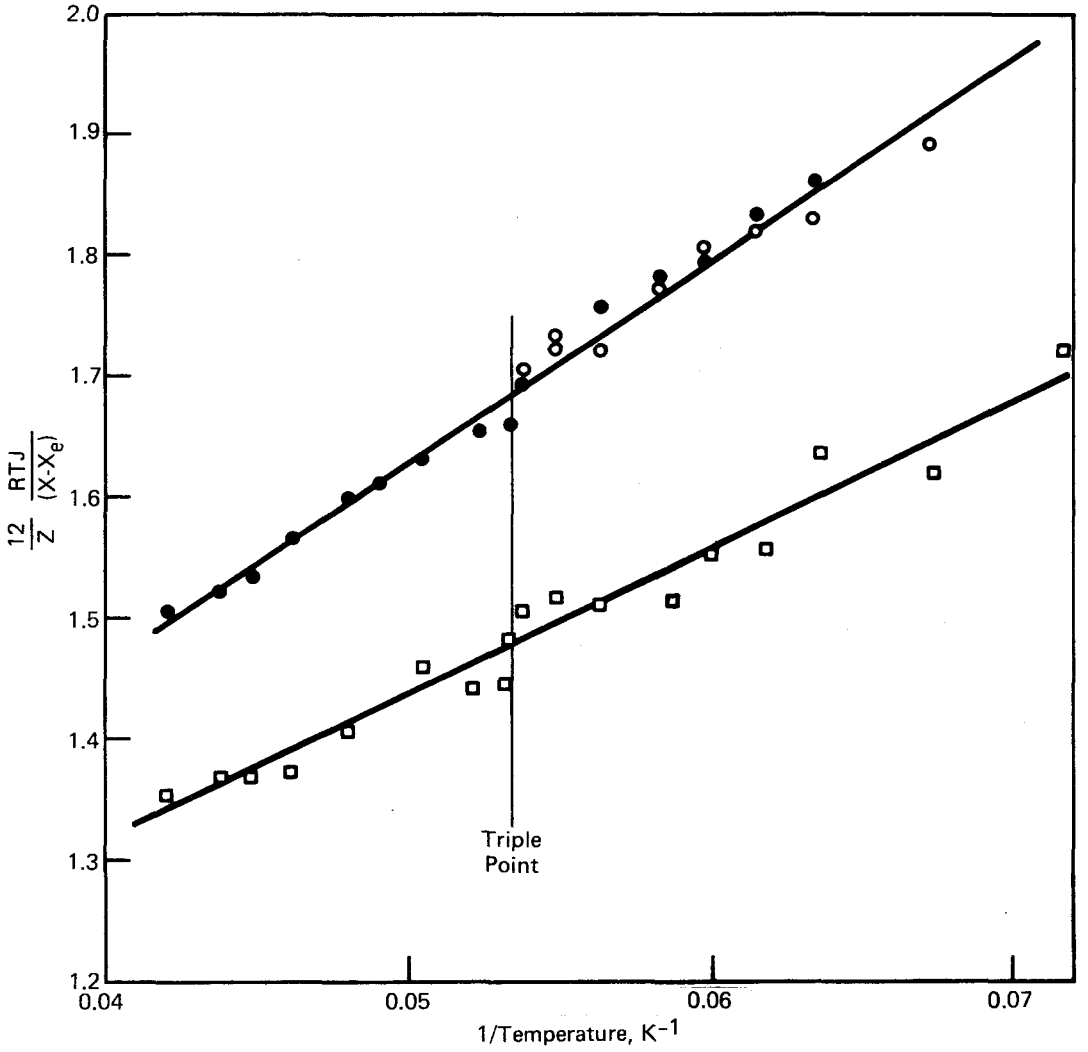

FIGURE I-8 - Display of experimentally determined quantity $RTJ/(X-X_e)$ normalized to 12 nearest neighbors in both the solid and the liquid.

Then from equation 5 the quantities in Table I-3 can be determined. A value of $Q_o = 0.135\text{Å}$ was determined in the work of L. Wolniewicz [9] and, if one assumes $r_o = 3.63$ is independent of temperature, one finds, as shown in Figure I-9, a slight temperature dependence for Q/Q_o. Previously determined values for Q/Q_o range from 0.83 to 0.99 with uncertainties of ± 0.05. The uncertainty in Q/Q_o in Figure I-9 is about 0.01 but depends on an accurate value of r_o.

Table I-3 - TEMPERATURE DEPENDENCE OF QUANTITIES IN EQUATIONS 5 AND 6

$\frac{1}{T}$	$\frac{\Lambda}{R}$	$\frac{\Gamma}{K}$	Q^2	Q/Q_o
0.042	0.506	0.962	1.49×10^{-34}	0.904
0.046	0.480	0.937	$1.45 \times$	0.895
0.050	0.472	0.929	$1.44 \times$	0.889
0.054	0.458	0.915	$1.42 \times$	0.882
0.058	0.452	0.909	$1.41 \times$	0.879
0.062	0.446	0.903	$1.40 \times$	0.876
0.066	0.439	0.896	$1.39 \times$	0.873
0.068	0.432	0.889	$1.38 \times$	0.870

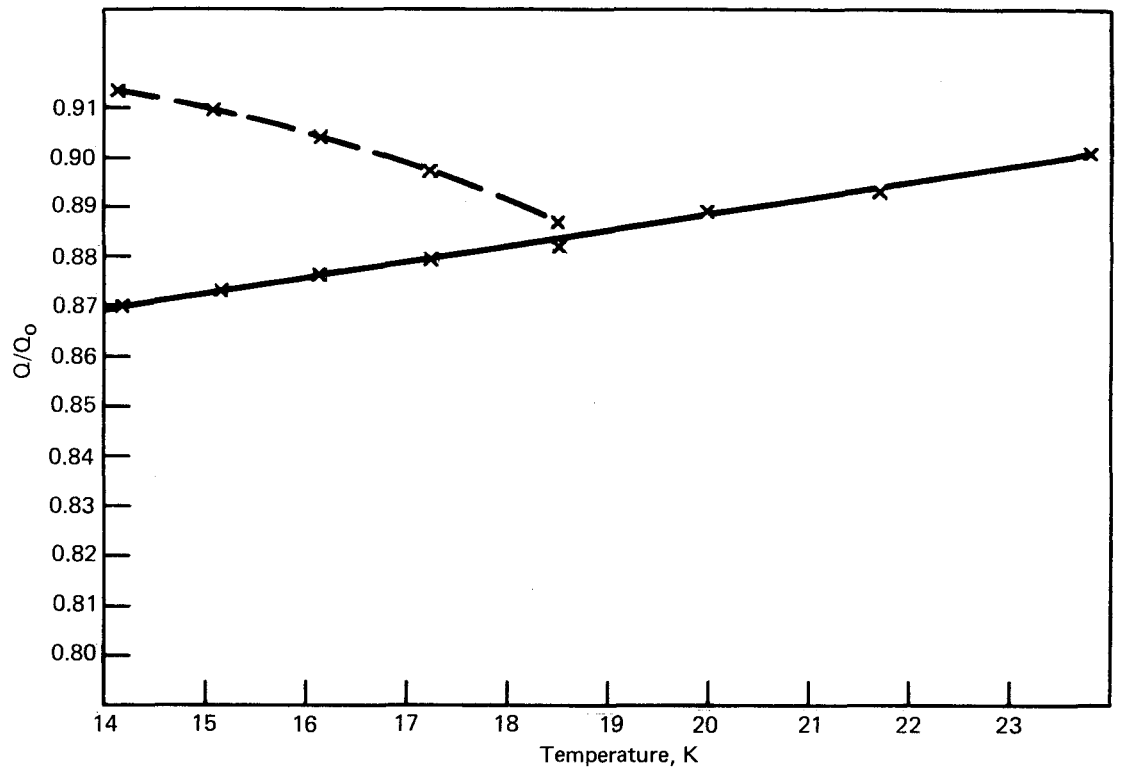

FIGURE I-9 - Apparent temperature dependence of the effective quadrupole moment, Q/Q_o.

The temperature dependence of the saturated density of solid D_2 has not been measured [10]. If one assumes $\ell n(\rho(0)/\rho(T)) = AT^5$ with $A = 1.48 \times 10^{-8}(K^{-5})$ and the molar volume at the triple point to be 20.48 (cc/mole), as done in Ref. 10, r_o varies between 3.60 and 3.70 in going from T = 14 K to 23.8 K. Using this variation in r_o in equation 5 and the experimental values of Λ/R, one arrives at the temperature dependence of Q/Q_o given by the dashed curve in Figure I-8. This temperature dependence is much larger than if r_o is constant and it is most likely based on an incorrect assumption about the temperature dependence of the solid density.

Hydrogen intermolecular potential function

G. T. McConville

In comparing several proposed potential functions to gaseous properties of H_2, we have found the differential scattering data of Farrar and Lee [11] could not be described with any of the potential functions [12]. It was then determined from Professor Lee that the collision energy which he gave as 2.71×10^{-14} erg was uncertain to 5%. Thus, scattering calculations were done using the H_2 HFD potential with the damping parameter D = 1.32 for scattering energies 3% and 5% higher than that given by Farrar and Lee. The results are shown in Figure I-10. A 3% higher scattering energy, which is within the uncertainty, using the HFD potential, is consistent with the data. This calculation clearly shows that the collision

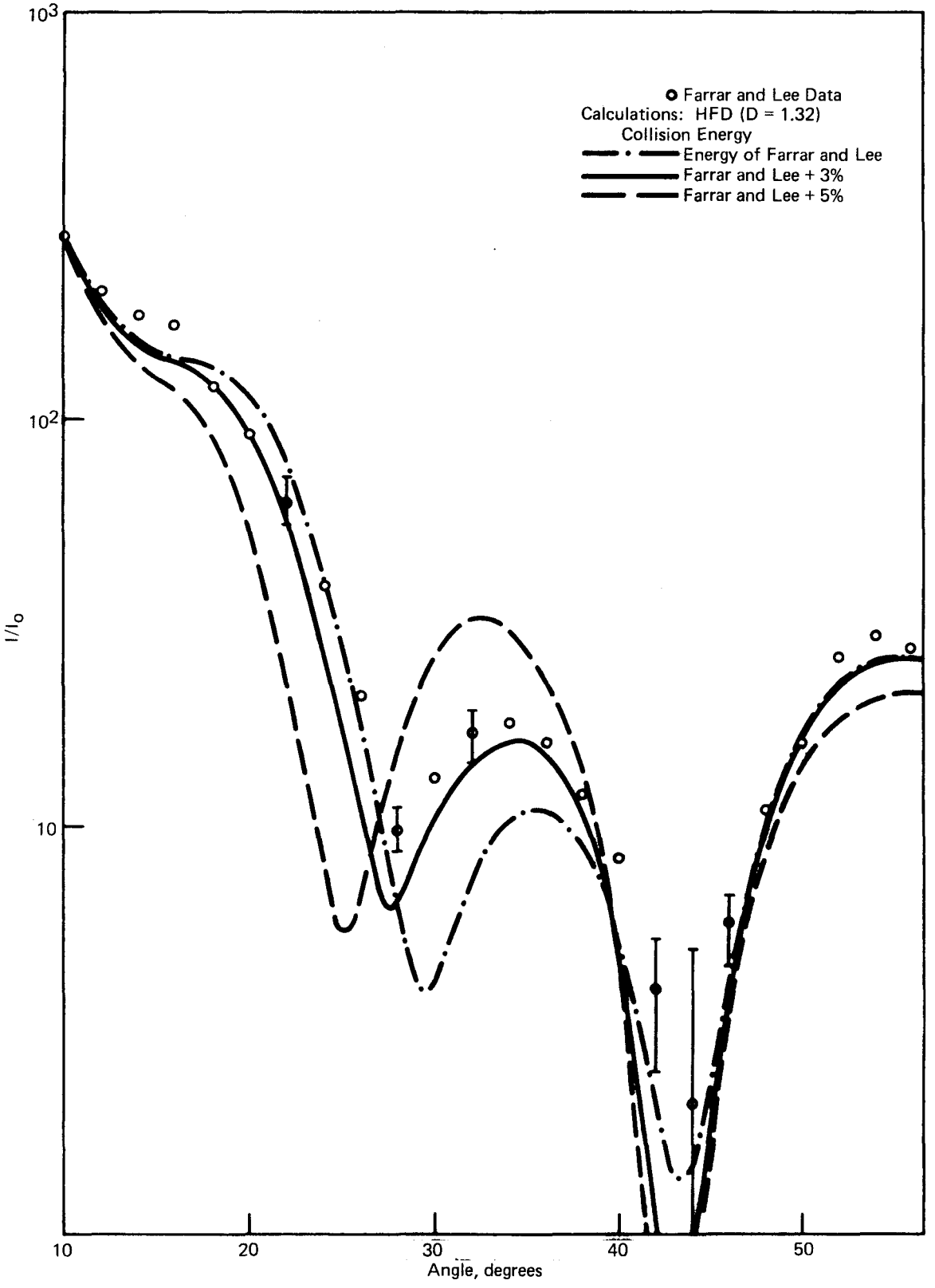

FIGURE I-10 - Dependence of the differential cross section of para H_2 on the collision energy.

energy must be known to 1% or better to discriminate between potential functions with differential scattering.

Low temperature trennschaukel

D. Cain and W. L. Taylor

Temperature instabilities and drift problems have been encountered in the constant temperature bath for the room temperature thermal conductivity gas analyzer system. Temperature stability is of primary importance in this application since the very properties of the thermistor sensors which make them so sensitive to changes in composition of gas mixtures also make them sensitive to temperature fluctuations. Thus, the Haake on-off thermo-regulator has been replaced with a proportional controller (YSI, Model 72) which powers a 1000 watt heater immersed in the bath liquid. The proportional controller is being used with a thermistor probe placed in the bath; the probe has a 0.3 second time constant and its resistance changes 100 Ω for every kelvin change in temperature from the chosen setpoint. With the controller set to its maximum sensitivity, the power to the heater changes 1% or more for every millikelvin change at the probe. A circulating pump and a stirrer, both directed from the heater toward the thermal conductivity analyzer cell, provide agitation to eliminate any gradients which might be present otherwise. With constant cooling primarily by evaporation (an external fan blows air onto the bath fluid surface) and heat proportional to the need of the system for maintenance of setpoint temperature, a passive resistance thermometer imbedded in the cell shows long-term temperature changes of $\pm$1 mK with short-term changes well within $\pm$0.5 mK.

Determining optimum operating conditions for the thermal conductivity bridge is largely a matter of trial-and-error, in part because the response of the sensors depends very much on cell geometry, length of leads, sealing materials and other factors. Ten to fifteen minutes is required for the bridge to stabilize after the gases are introduced and voltage is applied to the bridge. The first fluctuation observed is a change of one or two millidegrees in the temperature of the cell due to the temperature difference between the bath and the gas samples. This fluctuation dissipates quickly. Next, as voltage is applied, the bridge output oscillates wildly. A steady state is reached after several minutes, during which currents passing through the sensors cause them to self-heat. Resistance values of the thermistors vary, as heating and cooling due to thermal conduction into the medium come into balance, causing the initial oscillations in the bridge output.

Thermal conductivity bridges using thermistors as the sensing element are expected to exhibit a maximum output as a function of current to the bridge. This effect has been noted for this bridge. While this maximum represents a condition of greatest sensitivity of the bridge to the composition of gas mixtures, it is also a region of least stability with respect to current and temperature fluctuations. This instability is noted for the bridge beyond the maximum for the reasons noted above and as a consequence of the thermistors overheating. Indeed, if the current is increased beyond the value for maximum bridge output, the self-heating of the thermistors raises

the temperature of the cell above that of the bath fluid. The magnitude of this temperature rise is several millikelvin for extreme currents (10 mA or more).

The bridge output has also been found to be slightly dependent on the pressure of the gas samples being analyzed, even though the thermal conductivity of noble gases is not pressure sensitive at the pressures employed. This, again, attests to the sensitivity of these devices in a variety of parameters, as well as to the need for controlling them very carefully. A trade-off between the need for greater sensitivity to mixture composition and sample size may have to be made.

Finally, the dependence of the bridge output on the ambient temperature of the bath is under study. When this relationship is known, all of the parameters will be examined to arrive at optimum operating conditions for this bridge. The bridge output generated under these conditions as a function of mixture composition will represent the final calibration of the bridge.

II. Separation research

Liquid phase thermal diffusion

W. M. Rutherford

Experimental work on liquid phase thermal diffusion is continuing on the following topics: 1) measurement of isotopic thermal diffusion factors of selected compounds in a specially constructed, high precision column; 2) evaluation of parameters which influence nonideal behavior and parasitic circulation in columns with small hot to cold wall spacing; and 3) operation of an experimental liquid thermal diffusion cascade to develop techniques and a theoretical basis for separation of practical quantities of stable isotopes.

ISOTOPIC THERMAL DIFFUSION FACTORS

Isotopic thermal diffusion factors are determined by measurement of the isotopic separation under steady state and transient conditions. The apparatus and procedure for acquiring the necessary data have been described in previous reports [1,2]. According to the theory of the thermal diffusion column, the local concentration of component i as a function of time is given by:

$$\frac{\partial w_i}{\partial \Theta} = \frac{\partial}{\partial y}\left[w_i \sum_{i=1}^{n} m_{ij} w_j\right] + \frac{\partial^2 w_i}{\partial y} \qquad (1)$$

where w_i = mass fraction of component i,

$\Theta = \frac{Y_o H_o t}{\mu L}$ = dimensionless time,

$y = \frac{H_o z}{K}$ = dimensionless distance along column,

$m_{ij} = \frac{M_i - M_j}{M_i + M_j}$,

H_o = reduced initial transport coefficient, g/sec,

L = length of column, cm,

t = time, sec,

$Y_o = (\ln q_{Eij})/m_{ij}$,

$q_{Eij} = \frac{(w_i/w_j)_T}{(w_i w_j)_B}$ at equilibrium,

μ = distributed holdup, g/cm,

z = vertical coordinate, cm,

M_i = atomic or molecular mass.

A simplex optimization procedure has been developed to determine the values of H_o and H_o/K which best fit the data for a

given experiment. The associated computer program takes into account holdup at the ends of the column, and it makes adjustments for uncertainties in the effective starting time.

The theory of the column describes the relationship between the quantity H_o and the isotopic thermal diffusion factor, α_T. In precise terms, the quantity H_o is given by a complicated integral over the temperature range between the hot and cold walls of the column [3]; however, if certain simplified assumptions are made concerning the temperature dependence of the physical properties, then H_o is given with reasonable accuracy by:

$$H_o = \frac{-a^3 \rho g B (d\rho/dT)(\Delta T)^2}{6 \,:\, \eta \, \bar{T}} \alpha_o \qquad (2)$$

where α_o, the reduced thermal diffusion factor, is defined by

$$\alpha_o = \alpha_{Tij}/m_{ij}, \qquad (3)$$

and where α_{Tij} = isotopic thermal diffusion factor for the ij pair

a = hot to cold wall spacing,
B = circumference of column,
g = gravitational acceleration,
ΔT = temperature difference between hot and cold walls,
$\bar{T}$ = average temperature,
η = viscosity,
ρ = density.

In order to use Eq. 2 or its more complex and rigorous equivalent, it is necessary that the experimental column be free of parasitic effects or other nonideal phenomena. This can be determined by examining the agreement of the parameter K with theory. The experimental value of K is derived from measurement of the steady state separation thus:

$$\ln q_{Eij} = \frac{H_{ij} L}{K}$$

where

$$H_{ij} = H_o \, m_{ij}$$

L = length of column

The simple expression for K shows that it depends in a most sensitive way on the dimensions of the column and the physical properties of the fluid. Thus,

$$K = \frac{a^7 \rho^2 g^2 B (d\rho/dT)^2 (\Delta T)^2}{9 \,:\, \eta^2 \, D_{ij}}$$

where D_{ij} is the diffusion coefficient. Agreement between theoretical and experimental values of K is a necessary, but not sufficient, indication of a valid experiment.

Separation data were given in the previous report [1] for methyl chloride, ethyl chloride, 1-chloropropane and 1-chlorobutane. Additional data have now been acquired for ethyl bromide and 1-bromopropane.

Most of the measurements were at a hot to cold wall spacing of 254 μm; however, additional data were taken for 1-chloropropane at 305 μm and for ethyl bromide at 203 μm. Column dimensions and operating conditions for the several experiments are given in Table II-1.

The parameters derived from the data by simplex optimization are given in Table II-2. The fitting process worked well for most cases; however, some of the

Table II-1 - DIMENSIONS AND OPERATING CONDITIONS FOR LIQUID THERMAL DIFFUSION COLUMN EXPERIMENTS

Hot wall i.d.	13.87 mm
Hot wall o.d.	18.677 mm
	18.778 mm
	18.880 mm
Cold wall i.d.	19.286 mm
Water jacket i.d.	57.0 mm
Active length	456 mm
Steam temperature	164°C
Water temperature	14.4°C
Water flow rate	9.6 liters/min.

ethyl bromide data at 203 and 254 μm were of poor quality as the result of experimental difficulties with the purity and stability of the compound. The problem is illustrated in Figure II-1 which is a plot of the separation as a function of time for the experiments at 203 μm.

Experimental values of the coefficient H_{ij} were used to calculate the thermal diffusion factor for the ij pair for those experiments carried out at a spacing of 254 μm. The procedure for the calculation is outlined in Reference 3. It involves calculation of a coefficient ξ from theory where ξ is defined such that:

$$H_{ij} = \bar{\alpha}_{Tij} \xi$$

where $\bar{\alpha}_{Tij}$ is the average value of α_{Tij} over the temperature range from the hot wall to the cold wall of the column.

Physical properties for the six compounds as a function of temperature are required in order to calculate ξ and K from theory. These were compiled from standard sources, estimated, and extrapolated where necessary. Some of the values are highly uncertain. The viscosity of methyl chloride at high temperature is an example.

Table II-2 - EXPERIMENTAL AND THEORETICAL COEFFICIENTS FOR LIQUID PHASE THERMAL DIFFUSION EXPERIMENTS ON THE LOWER ALKYL HALIDES

	a, μm	$10^5 H_{ij}$, g/sec*		Kg-cm/sec		α_{Tij}*	α_o
		EXPT	Theory	EXPT	Theory		
Methyl chloride	254	24.9	-	0.0362	0.0262	0.0353	1.80
Ethyl chloride	254	19.6	-	0.0264	0.0147	0.0419	2.72
1-chloropropane	254	5.98	-	0.00628	0.00890	0.0196	1.55
	305	11.6	11.1	0.0266	0.0341		
1-chlorobutane	254	5.33	-	0.00578	0.00313	0.0350	3.26
Ethyl bromide	203	2.87	7.77	0.00350	0.00607		
	254	16.7	-	0.0570	0.0316	0.0220	2.39
	305	19.2	30.9	0.100	0.120		
1-bromopropane	254	5.84	-	0.0128	0.0136	0.0161	1.98

*for the $R^{35}Cl$-$R^{37}Cl$ and the $R^{79}Br$-$R^{81}Cl$ pairs

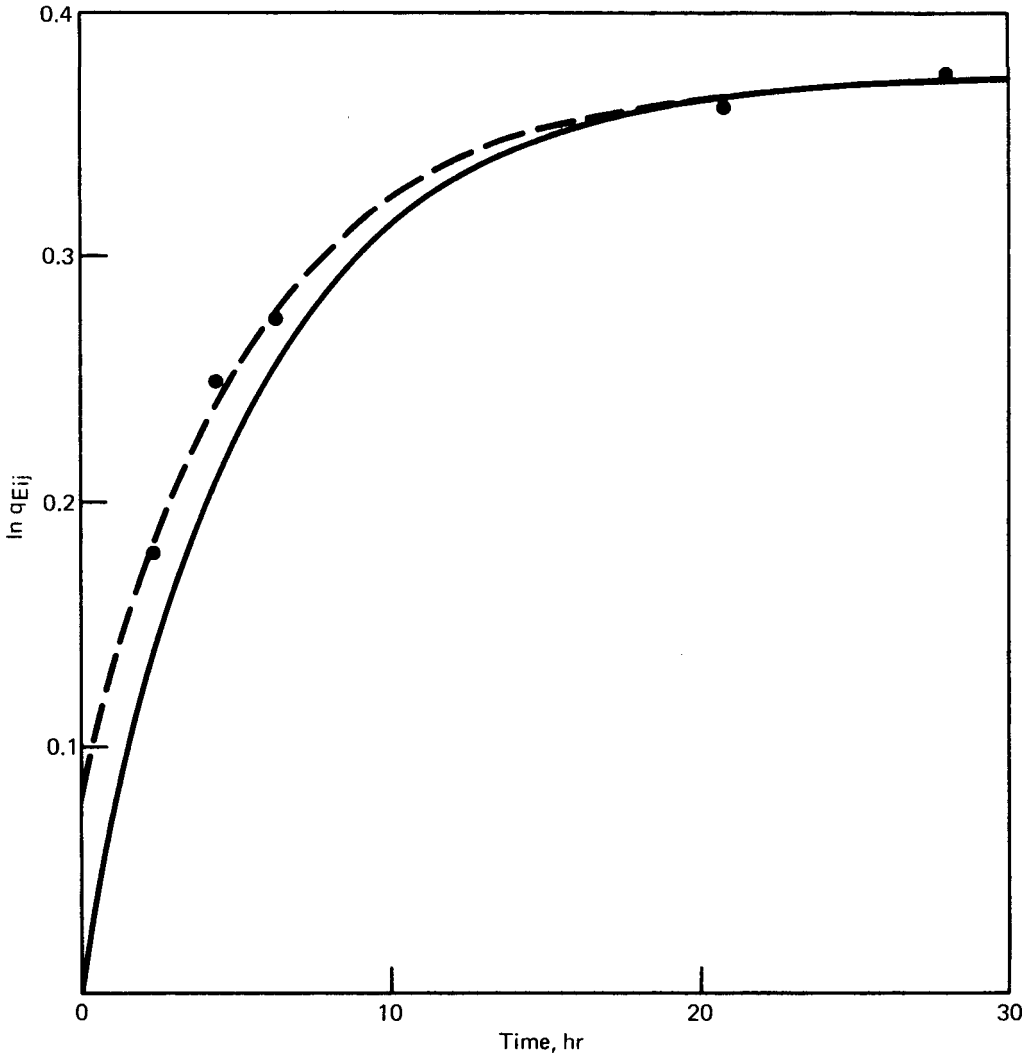

FIGURE II-1 - Isotopic separation of ethyl bromide in a 203 μm thermal diffusion column. The dashed curve is the best simplex fit to the data with a 1.15 hr displacement of starting time. The solid curve is constructed with the same parameters but without a time displacement.

The problems with the available data were discussed in detail in an earlier report [4].

The initial transport coefficient, H_{ij} was calculated from theory for those experiments which were done at a spacing other than 254 μm. The results are given in Table II-2 along with values of K calculated from theory for all experiments.

The agreement between experimental and theoretical values of K is not especially satisfying; therefore, the accuracy of the experimental values of α_{Tij} and α_o is limited to perhaps ±25%. It is believed that the results would be much better if the physical properties of these compounds were well known in the required temperature range.

CHLORINE ISOTOPE SEPARATION

The experimental 14 column liquid thermal diffusion cascade was used to separate a quantity of highly enriched chlorine-35. Parameters of the cascade and a description of the startup were given in the

previous report. The system, which uses methyl chloride as the working fluid, was set up for batch operation with a 475 g feed reservoir at the bottom and a 33 g product reservoir at the top. During 91 days of operation, material containing 230 g of chlorine-35 enriched to 99.6% was recovered from the cascade. This brings the total quantity of both chlorine isotopes separated by this technique to nearly 500 g.

A combustion apparatus was developed to oxidize the methyl chloride to HCl and CO_2. The accumulated enriched materials were processed to yield aqueous HCl which was subsequently neutralized with NaOH and evaporated to yield dry NaCl for storage and distribution.

Calcium isotope separation

W. M. Rutherford and K. W. Laughlin

Liquid phase thermal diffusion is being investigated as a means of separating calcium isotopes. A suitable compound for conventional liquid phase operation is not available; hence, it is necessary to use a solution of some calcium salt as a working fluid. A technique has been developed for selectively suppressing the separation of the salt from the solvent while the isotopic separation is allowed to proceed. The technique involves setting up a net flow of solvent in a direction counter to the direction of separation of solute. The theory of such a process was set forth in previous reports [5,6].

Experimental work on the separation of calcium isotopes by liquid phase thermal diffusion continued in the following areas: 1) development and testing of a new concept for setting up the solvent counterflow in the test column; 2) further development and testing of short columns (365 mm and shorter) to be used for evaluating isotope effects in the absence of solvent counterflow; 3) testing of experimental and analytical techniques on the isotopic separation of an aqueous lithium nitrate solution; and 4) measurement of physical properties of concentrated $Ca(NO_3)_2$ solutions.

SOLVENT FLOW EXPERIMENTS

The concept of solvent counterflow originally developed by Korsching [7] calls for the continuous, controlled injection of pure solvent at the bottom of the experimental column and removal of the solvent by distillation at the top. Our first effort [6] to set up such an experiment was not successful, in part because of the development of unstable density gradients in the column, but also in part because of the poor mechanical performance of the distillation apparatus.

A new method was devised to set up the required conditions without the use of a distillation apparatus (or boiler) to remove solvent at the top of the column. The concept is illustrated in Figure II-2. Solvent evaporation is replaced by continuous feed to the top of the column of a concentrated solution of material of natural isotopic abundance in conjunction with the continuous withdrawal of relatively more dilute material from the same location. If allowed to proceed indefinitely, this would lead to the following: 1) the isotopic composition at the top of the column would approach natural abundance and 2) the solute concentration at the top would assume a value consistent with the material balance on the several flows.

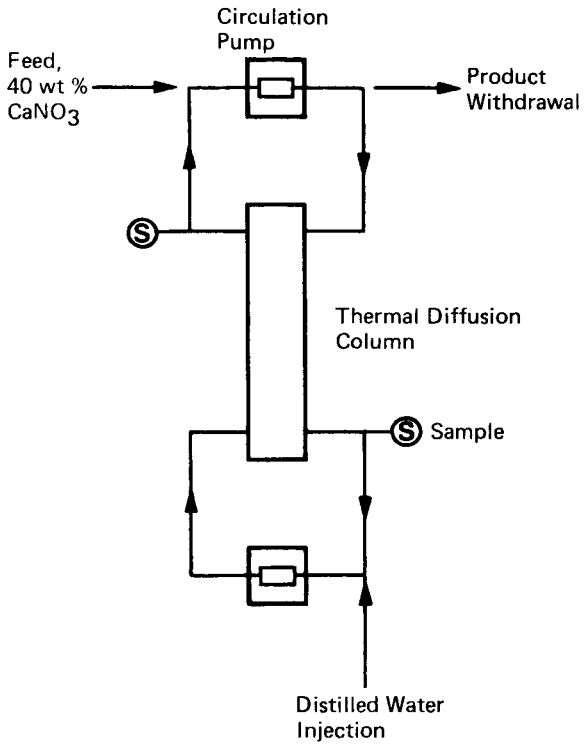

FIGURE II-2 - Simplified schematic of the experimental setup for measurement of Ca isotope separation with solvent injection.

Three experiments were done with this configuration. The experimental column and operating conditions were the same as those reported in Reference 5: length, 720 mm; annular diameter, 25 mm; hot-to-cold wall spacing, 254 μm; steam temperature, 164°C; cooling water temperature, 25°C.

For the first experiment, the column was filled with a 10% by weight aqueous solution of $Ca(NO_3)_2$. Separation was allowed to proceed for several hours without external flow in order to establish a stable density gradient. Then the several flows were established at the following values: 1) solvent (water) feed to the bottom of the column, 0.24 g/hr; 2) 40% solution feed to the top of the column, 0.11 g/hr; 3) top outflow, 0.35 g/hr. We attempted to hold these conditions steady for the next 14 days; however, some variation was unavoidable, and this may have amounted to as much as ±20% on the feed rate of concentrated solution.

Solute concentrations during the experiment are shown in Figure II-3 along with values calculated from finite difference solution of the time dependent transport equation (8):

$$\frac{\partial w_1}{\partial t} = -\frac{1}{\mu}\frac{\partial \tau_1}{\partial z} \qquad (1)$$

where w_1 is the solvent mass fraction, t is time, and μ is column holdup per unit length.

In order to model the observed behavior theoretically, it was necessary to use values of H_{ss}, the initial transport coefficient for the solute-solvent pair, somewhat smaller than the estimates derived from earlier experiments without counterflow [6]. This is not particularly surprising in view of the crude nature of the procedure used to generate the earlier data.

The solvent injection rate was set below that required to completely offset the solute concentration gradient; however, it was sufficient to sustain a useful solute concentration at the top of the column.

Samples were taken for calcium isotope ratio determinations on days 12, 13, and 14. The results are given in Table II-3. The isotopic separation is, as expected, mass dependent with the separation of the ^{40}Ca-^{48}Ca pair showing the largest effect. The effect is similar in magnitude to isotope effects obtained without

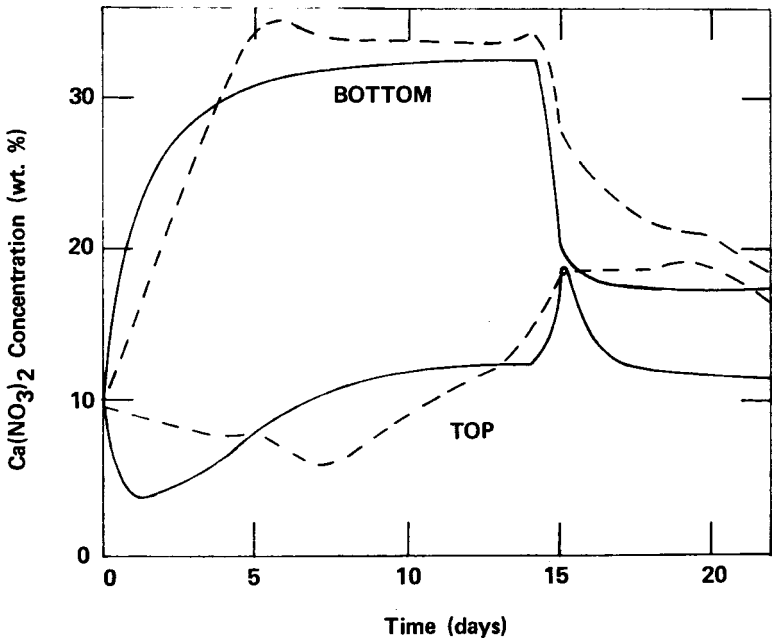

FIGURE II-3 - Solute concentration during the first Ca isotope separation solvent flow experiment. The dashed lines are experimental data; the solid lines are calculated from the solution of Eq. 1.

Table II-3 - SEPARATION, DURING THE FIRST COUNTERFLOW EXPERIMENT, OF Ca ISOTOPES IN AN AQUEOUS SOLUTION OF $Ca(NO_3)_2$. THE DESIGNATIONS T AND B REFER TO SAMPLES TAKEN FROM TOP AND BOTTOM, RESPECTIVELY

Time (days)		Isotopic Composition (at. %) ^{42}Ca	^{43}Ca	^{44}Ca	^{48}Ca	ln q_{48}*
Standard		0.62	0.125	1.88	0.152	
	Solvent Flow: 0.24 ml/hr; feed flow, 0.08 ml/hr					
12	T	0.60	0.117	1.78	0.136	0.211
	B	0.64	0.134	2.00	0.168	
13	T	0.60	0.120	1.77	0.135	0.231
	B	0.64	0.136	2.01	0.170	
14	T	0.60	0.123	1.77	0.137	0.233
	B	0.64	0.133	2.02	0.173	
	Solvent Flow: 0.60 ml/hr; feed flow, 0.18 ml/hr					
18	T	0.62	0.128	1.88	0.151	0.148
	B	0.64	0.133	2.01	0.175	
19	T	0.63	0.129	1.89	0.152	0.125
	B	0.64	0.132	2.00	0.172	
20	T	0.61	0.127	1.87	0.153	0.134
	B	0.64	0.132	2.02	0.175	
21	T	0.62	0.128	1.87	0.150	0.148
	B	0.64	0.134	2.02	0.174	
23	T	0.62	0.128	1.87	0.150	0.166
	B	0.64	0.132	2.04	0.177	

*q_{48} is the separation factor for the 40-48 pair.

solvent injection in aqueous solutions of other elements [9-13]. The effect seems to be large enough to support separation of calcium isotopes on a practical scale using the solvent flow technique.

An attempt to reduce the solute concentration gradient by increasing solvent flow was only partially successful. On day 14 of the experiment the flow rates were increased to the following values: solvent feed, 0.60 g/hr; 40% solution feed, 0.25 g/hr; top outflow, 0.85 g/hr. As indicated in Figure II-3, the solute concentration gradient did decrease, but the results were somewhat out of line with those predicted. A detailed examination of the composition profiles calculated from theory showed that a clearly defined, positive concentration gradient would develop during the transition period following the change in conditions. This would be expected to lead to at least a partial remixing of the column contents. As expected under these conditions, the isotope separation dropped somewhat. The results are equivalent to an average separation factor of 1.16 for the ^{40}Ca-^{48}Ca pair as opposed to the value of 1.26 obtained during the first 14 days of the experiment.

The second and third solvent counterflow experiments of this series were run with a somewhat modified arrangement of the feed and withdrawal systems at the top of the column. The modification increased the flexibility of the system so that the feed rate of 40% solution could be more readily adjusted to avoid density inversions in the column.

Results of the two experiments are compiled in Table II-4. It was possible to sustain concentrations at a higher level during these runs, and isotopic separation factors were comparable to those observed during the first run. Both runs, however, were plagued by persistent mechanical problems with the solvent injection pump. The resulting instability in solute concentrations would be expected to degrade the isotopic separation and to preclude any hope of interpreting the transient character of the isotopic separation.

It is interesting to note that in the latter part of the third experiment, the isotopic separation was essentially obliterated by a deliberately induced concentration and density inversion in the column. This result confirms our previous speculation about the effect of such inversions.

EXPERIMENTS WITHOUT SOLVENT FLOW

A short column similar in characteristics to the one used for solvent flow experiments, but 365 mm instead of 720 mm in length, had been constructed for the measurement of isotopic separation without solvent counterflow. Our estimates indicated that the $Ca(NO_3)_2$-water separation in a column of this length would be small enough to leave the concentration of solute in the top at a level high enough for accurate determination of the isotopic composition. Results given in the last report [14], however, were erratic and a significant isotopic separation could be found only in the case for which D_2O was used as solvent instead of H_2O.

Additional analytical work on top samples from the 365 mm column now suggests that solute concentrations were much lower than we had previously reported. A precise evaluation of solute concentration

Table II-4 - SOLUTE CONCENTRATIONS AND THE SEPARATION OF ^{48}Ca DURING THE SECOND AND THIRD COUNTERFLOW EXPERIMENTS

Time (days)	Solute Concentration (wt %) Top	Bottom	$\ln q_{48}$
Experiment 2:	Solvent flow, 0.242 ml/hr; feed flow, 0.137 ml/hr		
5	3.71	33.4	0.079
6	5.20	30.3	0.041
7	6.17	27.3	0.103
8	Change feed flow to 0.275 ml/hr		
11	13.0	35.4	0.130
13	18.6	37.1	0.212
15	21.8	36.9	0.169
Experiment 3:	Solvent flow, 0.242 ml/hr; feed flow, 0.275 ml/hr		
14	22.9	36.8	0.215
17	Change solvent flow to 0.603 ml/hr feed flow to 0.687 ml/hr		
19	24.3	23.9	0.038
20	23.4	22.7	-0.022
21	23.9	21.7	0.034

is not possible because the amount of sample available is very small; hence, separate experiments must be run to obtain material for both solute and isotopic analyses. The results for several samples analyzed for $Ca(NO_3)_2$ by different techniques are given in Table II-5. Each sample represents a different experiment; thus, the results cannot be construed as a comparison of techniques. The results do suggest, however, that actual solute concentrations could easily have been as low as 1 ppm.

Table II-5 - SOLUTE CONCENTRATIONS FOR LIQUID PHASE THERMAL DIFFUSION EXPERIMENTS WITH $Ca(NO_3)_2$-H_2O SOLUTIONS IN A 365 mm COLUMN

Technique	$Ca(NO_3)_2$ Concentration (ppm)
Refractive Index	1200
Emission Spectrometer	2000
Anion Chromatography (by NO_3)	0.9
Spark Source Mass Spectrometer	60

System length was further reduced by the construction of another column of the same cross section but with a total length of 150 mm. Two experiments have now been completed in the new device. The results, which were obtained with an initial fill composition of 10%, are given in Table II-6 and Figure II-4. There was a moderate leak in the column

Table II-6 - SOLUTE CONCENTRATIONS AND THE SEPARATION OF ^{48}Ca IN LIQUID THERMAL DIFFUSION EXPERIMENTS IN A 150 mm COLUMN WITHOUT SOLVENT FLOW

Time (days)	$Ca(NO_3)_2$ Concentration (wt %) Top	Bottom	ln q_{48}
Experiment 1			
4	0.92	19.8	0.146
5	1.37	10.4	0.122
10	3.57	16.8	0.028
Experiment 2			
4	0.66	20.3	-
5	<0.1	20.7	-
6	<0.1	20.8	-

during the first experiment which accounts for the decrease of the separation with time. Experiment 2, which was run after the leak was repaired, resulted in a much larger separation factor for the solute solvent system. After an elapsed time of somewhat more than 100 hr, it was not possible to distinguish between the top sample and distilled water on the basis of 50 µL samples. Several larger sample sets were collected, however, by successive removals of the contents of the top circulation loop with intervening periods of several days to reestablish the concentration distribution. These will be analyzed by ion chromatography or by specific ion electrode. If sufficient calcium is present, the samples will be submitted for isotope ratio determination.

LITHIUM ISOTOPE SEPARATION

A short experimental series was run to test performance of the 365 mm column with a solution which was known to give an isotopic separation without an

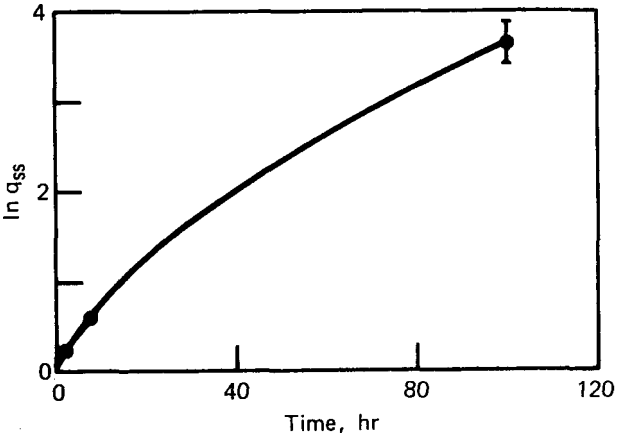

FIGURE II-4 - Separation of $Ca(NO_3)_2$ from H_2O in the 150 mm liquid phase thermal diffusion column.

accompanying large solute-solvent separation. Panson [11] found significant isotopic separations by liquid phase thermal diffusion of $LiNO_3$ solutions up to 5M in a 250 mm column.

The 365 mm column was filled with a 5 wt % solution of $LiNO_3$ in H_2O. Separation was allowed to proceed until nearly steady concentrations of 2.2 and 8.3% $LiNO_3$ were reached at the top and bottom of the column, respectively. Samples were removed and submitted to ORNL for isotopic ratio determination. The procedure was repeated 3 times for 3 separate determinations of the isotopic separation factor between ^6Li and ^7Li. This was found to be 1.159 $\pm$ 0.002 and of the same order of magnitude as Panson's results. There appears, therefore, to be no basic

problem with the 365 mm column or with the experimental procedure.

PHYSICAL PROPERTIES OF $Ca(NO_3)_2$ SOLUTIONS

It is important to be able to calculate column performance from theory so that reasonably accurate predictions can be made of the potential productivity of calcium isotope separation cascades. The theoretical calculations require knowledge of the density, viscosity, thermal conductivity and diffusion coefficient as functions of temperature over the temperature range from the cold wall to the hot wall of the column. Under our standard operating conditions the hot wall temperature is in the 140 to 160°C range. Literature data, if available at all, are seldom given over a broad temperature range. It seemed advisable, therefore, to measure at least density and viscosity of the $Ca(NO_3)_2$-H_2O system over a broad temperature range.

Density measurements were made for 25 and 40 wt % solutions with a quartz pycnometer over the temperature range from 20 to 95°C. Viscosity measurements were made for the same solutions over the same temperature range with a Zeitfuch cross-arm viscometer calibrated at 20° and 45°C with degassed, distilled water. The viscometer constant was 0.002972 ± 0.000004 centistoke/second.

Results for both parameters were interpolated to even temperatures and are given in Table II-7.

Table II-7 - DENSITY AND VISCOSITY OF AQUEOUS $Ca(NO_3)_2$ SOLUTIONS

Temperature (°C)	Density (g/ml)		Viscosity (cP)	
	25 (wt %)	40 (wt %)	25 (wt %)	40 (wt %)
20	1.2134	1.3725	1.771	3.724
25	1.2118	1.3688	1.606	3.341
30	1.2101	1.3651	1.454	2.993
35	1.2082	1.3612	1.317	2.681
40	1.2059	1.3574	1.194	2.408
45	1.2035	1.3535	1.085	2.193
50	1.2009	1.3496	1.007	1.999
55	1.1980	1.3457	0.9346	1.825
60	1.1950	1.3418	0.8685	1.672
65	1.1918	1.3379	0.8085	1.546
70	1.1884	1.3339	0.7545	1.445
75	1.1849	1.3299	0.7066	1.354
80	1.1811	1.3258	0.6647	1.275
85	1.1773	1.3217	0.6288	1.207
90	1.1733	1.3176	0.5991	1.149
95	1.1691	1.3135	0.5753	1.102

Calcium chemical exchange

B. E. Jepson and G. C. Shockey

Lithium isotope effects in chemical exchange with cryptands have been reported previously [15]. This work found that exchange with cryptands yielded significant isotope effects, and work on calcium chemical exchange with cryptands was undertaken. Calcium cryptates were found to be highly water soluble, and two-phase liquid-liquid chemical exchange systems utilizing an aqueous phase were not feasible. Cryptands can, however, be chemically bound to solid resin support materials to permit chromatographic separations. Heuman and Schiefer recently reported single-stage separation factors (α) in calcium exchange with resin-bound 222B cryptand [16]. On a per mass unit basis their results yielded separation factors as large as $\alpha = 1.0015$, a substantial increase over separation factors normally found in calcium ion exchange chromatography.

Calcium ion distribution measurements were made for several solvent combinations and an ethanol/0.1 M water fluid phase was selected for column work which is now in progress. The breakthrough technique was used for a first run; however, isotope analyses are not yet available. The calcium breakthrough in this run occurred approximately at the time predicted by the absorption isotherm developed for this solvent system indicating that calcium phase distribution was favorable.

Mutual diffusion

D. Cain and W. L. Taylor

Efforts to characterize the temperature dependence of the mutual diffusion coefficients of binary noble gas mixtures continue. In a previous report [17] we presented the results of experiments on the interdiffusion of argon with helium, neon and xenon. We also presented the findings of detailed checks of our experimental procedures and equipment. These failed to uncover any procedural problems with the experiments. Nevertheless, data for the system argon-helium showed quantitative disagreement with the results of other experimenters and with theoretical calculations as well as a great deal of internal scatter. Perusal of laboratory manuals and mass spectrometer printouts turned up errors in the normalization of some of the gas concentrations which enter into the calculations. In addition, some experiments were found to have been contaminated with air and the results were discarded. Finally, corrections were applied to mass spectrometer results which account for the different pumping speeds of the components of a gas mixture [18].

All of these factors slightly change the mixture compositions from which the diffusion coefficients, D_{12}, are calculated. Since the diffusion coefficients are very sensitive to these compositions, the changes in the gas analyses have changed the appearance of the data significantly. The revised data for argon-helium from the last report [17] along with new data obtained from experiments performed in this reporting period are listed in Table II-8.

Table II-8 - DIFFUSION COEFFICIENTS OF ARGON-HELIUM AT ONE ATMOSPHERE PRESSURE, EQUIMOLAR EQUILIBRIUM CONCENTRATION

Temperature (K)	D_{12} (cm^2/sec)
358	1.044
403	1.264
500	1.799
570	2.2698
646	2.723
653	2.850
790	3.933
799	4.188
871	4.680
941	5.333
1021	6.130
1089	7.007
1172	7.891
1248	9.121
1249	8.884
1252	9.080
1292	9.347
1305	9.235
1306	9.583
1357	10.316

Figure II-5 shows the present data along with other recent data found in the literature [19-22] on a deviation plot. The base line of the plot represents values of the diffusion coefficient for this system calculated from the expression given by Marrero and Mason [23] for the value of D_{12} as a function of temperature. This expression was obtained through the compilation of all the experimental data available to those authors at the time. The symbols in Figure II-5 represent data which have become available since the compilation of Marrero and Mason. The dashed lines on either side of the base line are the uncertainties of the correlating functions. Also shown (dash-dot curve) is the deviation from the correlating function of D_{12} values obtained from viscosity data through the use of mutual consistency relations [17]. This analysis is based on the validity of the theory of corresponding states.

As can be seen from the figure, significant discrepancies exist in the body of data available. The base line of the deviation plot is not meant to represent the "true" values of D_{12}; it represents all the experimental data reported before those shown by the symbols and should include the "true" value within its uncertainty limits. Many of the sets of data are seen to not agree with the Marrero and Mason correlation, even to within their mutual uncertainties.

The present data and those of Hogervorst [19] are the only recent measurements of D_{12} above 800 K. We have spent a considerable amount of time investigating the discrepancy between his data and ours, as this property is of great usefulness in characterizing the interaction potentials of the component species of a binary mixture. Figure II-5 shows that our data lie for the most part within the uncertainty limits set by Marrero and Mason and agree over the entire temperature range to within the mutual uncertainties of the data. Hogervorst, on the other hand, agrees to within the mutual uncertainties of his data with that of the present data and with that of the correlation only at low temperatures. We feel that his data are increasingly lower than the "true" values and, thus, in error. This view has been supported by other investigators, both for this system [24] and others [25]. R. A. Aziz [26] has suggested that the "true" values

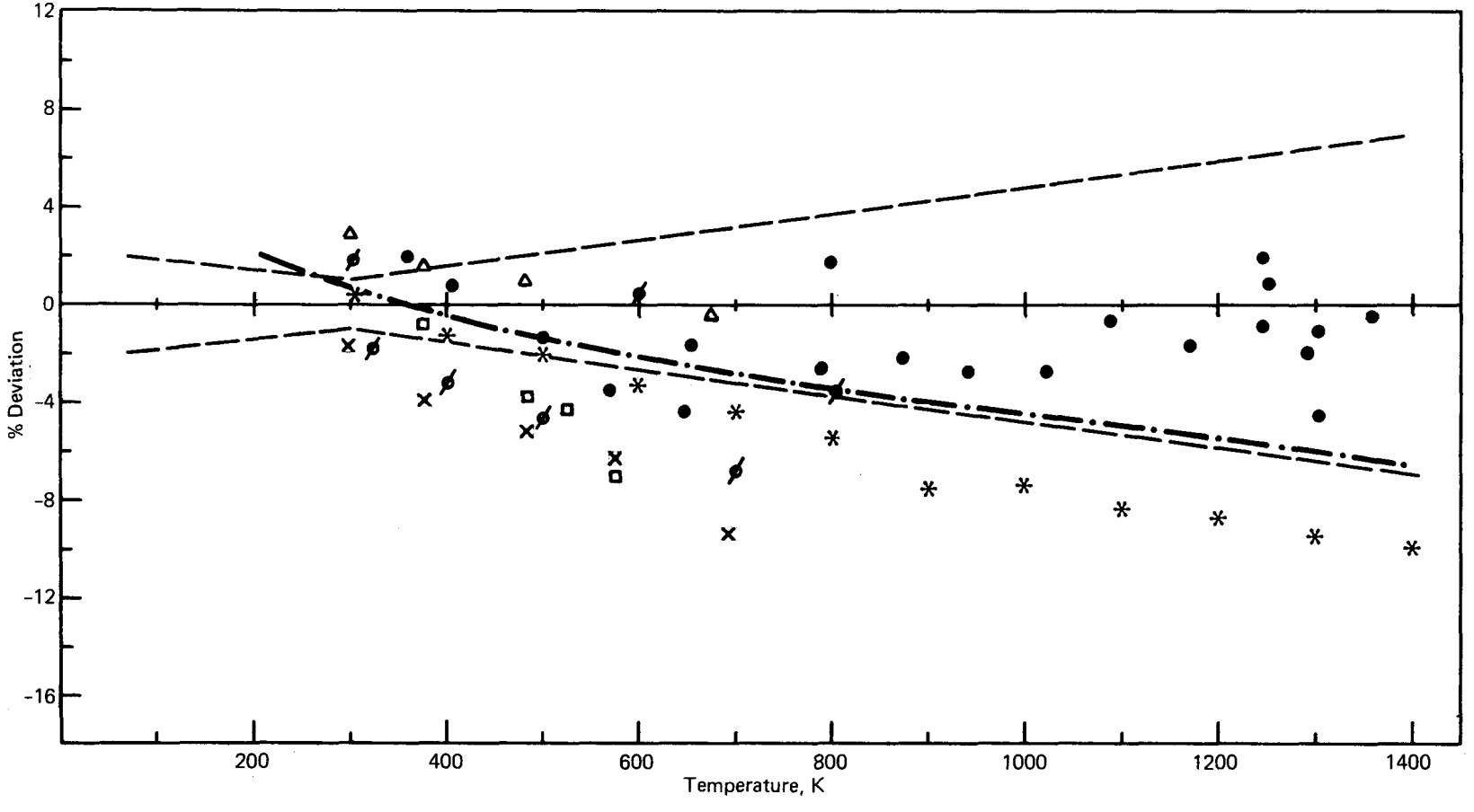

FIGURE II-5 - Percentage deviation of argon-helium diffusion coefficients from the Marrero and Mason correlating function [23]. The experimental points are: •, present results; *, Hogervorst [19]; □, Suetin, et al, glass capillary [20]; X, Suetin, et al, metal capillary [20]; Δ, Kalinen and Suetin [21]; ϕ, Liner and Weissman [22]. The curves are: ---, uncertainty limits for Marrero and Mason correlating function [23]; -·-·-, D_{12} values derived from viscosity data [17].

of D_{12} lie in between the values given by the correlating function and those determined by Hogervorst; the present data would seem to support this notion.

Theoretical calculations will now be compared with the present argon-helium experimental results. A similar examination of the raw experimental data is under way for argon with neon and xenon (i.e., normalization and mass spectrometer corrections for different pumping speeds). Also, additional experiments have been run on the argon-neon system because some of the experiments were contaminated with air; analysis of these results is not yet complete.

Molecular beam scattering

R. W. York and W. L. Taylor

DIMER RATIO MEASUREMENTS

Dimer ratio measurements have been made for neon nozzle beams at nine different beam source temperatures using the quadrupole detection system. Information on the dimer content in the beam is necessary for accurate corrections to measured cross section values [27]. The measured cross sections appear too large when there exists a significant dimer fraction in the beam, since the dimer is roughly twice the size of the monomer. The neon dimer is one of the so-called "van der Waals" dimers in which the two neon atoms are weakly bound together by van der Waals forces and do not share any electrons. Even though these dimer atoms are weakly bound, they can, under certain conditions, reach substantial concentrations in the small supersonic nozzle jets used as molecular beam sources.

Accurate measurements of beam dimer content are difficult to make, without information on the dimer history, owing to the fragmentation of fragile dimer atoms in the ionizer into the parent monomers. The finite inevitability of some ionizer fragmentation causes the most accurate dimer measurements to give at best a "minimum" beam dimer concentration.

Three different ionizer electron energies were used to investigate this dimer dissociation. The lowest electron energy used (38.5eV) was just under the second ionization potential for neon (40.9eV). This was the minimum electron energy which, for our detector system, would produce a usable quadrupole output signal. Electron energies of 50eV and 60eV were used for comparison to the results at 38.5eV to show increasing dimer fragmentation with electron energy.

A sensitivity correction must be made to the measured mass ratio, in this case mass-40/mass-20. Here, mass-20 is the neon monomer mass and mass-40 is the dimer mass. The relative sensitivity of the detector to these masses must be determined. When stable species are involved, it is usually a straight forward procedure to make up samples of known composition for such a calibration. This option is not available in our situation because of the instability of the weak van der Waals forces holding the neon atoms together.

We used a 50/50 mixture of argon-40 and neon-20 for the measurement of the mass-40/mass-20 sensitivity factor, substituting argon-40 for the neon dimer mass. The results of this measurement had to be corrected for the doubly ionized argon-40

which would be detected as mass-20. Mass-40 and mass-20 peak heights were measured using an argon background with no neon present. Here,

$$\text{mass-40} = {}^{40}Ar^{+} \text{ (singly ionized)}$$
$$\text{mass-20} = {}^{40}Ar^{++} \text{ (doubly ionized)}$$

From this measurement, the doubly ionized correction factor is,

$$f = \frac{\text{mass-20}}{\text{mass-40}} = \frac{{}^{40}Ar^{++}}{{}^{40}Ar^{+}} \qquad (1)$$

Once f is determined, all instrument settings remain fixed and the sensitivity factor K is measured using a 50/50 mixture of $^{20}Ne/^{40}Ar$. The mass-20 and mass-40 peak heights are again measured. Here,

$$\text{mass-40} = {}^{40}Ar^{+}$$
$$\text{mass-20} = {}^{20}Ne^{+}+{}^{40}Ar^{++}$$

Substituting $^{40}Ar^{++} = f\,^{40}Ar^{+}$ from equation (1), the sensitivity correction factor is,

$$K = \frac{{}^{20}Ne^{+}}{{}^{40}Ar^{+}} = \frac{\text{mass-20}}{\text{mass-40}} - f \qquad (2)$$

Then, using a neon beam, the mass-20 and mass-40 peak heights are measured. Here,

$$\text{mass-20} = {}^{20}Ne^{+} \text{ (monomer)}$$
$$\text{mass-40} = {}^{20}Ne_2^{+} \text{ (dimer)}$$

The corrected dimer ratio is then,

$$R_D = K\,\frac{\text{mass-40}}{\text{mass-20}} \qquad (3)$$

Presently, seventeen of the scheduled twenty-two neon dimer experiments have been completed. The experimental data will be reduced upon completion of the experiments and the foregoing correction applied. Thus far, it appears that, for the neon beam system, the operating conditions used in the Ne-Ar total cross section measurements recently presented at the Twelfth Rarefied Gas Dynamics Symposium [28] were adequate to limit the dimer fraction to the estimated 0.5%.

HELIUM-ARGON TOTAL SCATTERING CROSS SECTIONS

Experimental data for the total scattering cross sections of helium-argon have been reduced to account for the finite angular resolution in the apparatus. This correction occurs because some beam atoms which undergo scattering in the target cell will still enter the detector and be counted as part of the attenuated beam. Thus, the reduced cross section, normally designated as Q_{exp}, is too low by an amount, ΔQ. The "effective" cross section is thus simply,

$$Q_{eff} = Q_{exp} + \Delta Q$$

where ΔQ was calculated for each experiment by the procedure given in Ref. 29. There were, however, typographical errors in two equations given in Ref. 29 and these are given correctly below.

1) Intensity distribution function for $r_k<r<r_s$.

$$i(r) = \frac{1}{\pi(r_s-r_k)^2}\left[(r_s+r_k)^2 \arccos\left\{\frac{r^2+r_sr_k}{r(r_s+r_k)}\right\}\right.$$
$$+ (r_s-r_k)^2 \arccos\left\{\frac{r^2-r_sr_k}{r(r_s-r_k)}\right\}$$
$$\left.-2\left\{r^2(r_s+r_k)^2 - (r^2+r_sr_k)^2\right\}^{\frac{1}{2}}\right]$$

2) Angular distribution correction.

$$\Delta Q = (0.175/\pi)\int_{o}^{\theta 1} [W(\theta)(Q_{eff}^2/Fa_0^2)$$

$$x\, k_1^2(1+0.56/X^2)\exp\{-0.7(\theta/\theta^*)\}]\theta d\theta$$

where

$$(1/\theta^*)^2 = (0.193/\pi)(Q_{eff}/Fa_0)k_1^2(1+0.40/X^2).$$

The effective cross section is plotted as a function of the beam velocity in Figure II-6. The solid circles represent a helium beam scattered by an argon target gas while the solid triangles represent the "inverse" experiment. Unfortunately, it was not feasible to overlap the beam velocities and it is impossible to determine whether or not the solid triangles form a true extrapolation of the curve determined by the solid circles. The resolution corrections were very small for the helium beam but approximately two orders of magnitude larger, and certainly non-negligible, for the argon beam. The data are summarized in Table II-9.

In order to account for the effect of velocity distributions in the beam and target gas, an average relative speed must be assigned to the measured cross section. As in our previous work, the beam is assumed to be monoenergetic (mach number $\cong$45 for helium) and the target gas is assumed to have a Maxwellian velocity distribution. With these assumptions, the deconvolution procedure was carried out as described in Ref. 27. The deconvolution process made only a small change for the helium beam/argon target but considerably affected the cross sections for the inverse experiments. The deconvoluted cross section Q^{II}, is plotted as a function of the average relative velocity, $\bar{V}_r$, in Figure II-7, and the deconvolution integrals and resulting cross sections are listed in Table II-10.

The Wentzel-Kramers-Brillouin (WKB) approximation was used to calculate phase shifts which in turn were summed over all angular momenta to arrive at a theoretical prediction for the cross sections. An intermolecular potential of the Hartree-Fock-Dispersion (HFD) functional form recommended by Aziz, et al [30] was utilized.

$$V(r) = A\exp(-\alpha r) - (C_6 r^{-6} + C_8 r^{-8} + C_{10} r^{-10})D(r).$$

$$D(r) = \exp[-(1.28r_m/r-1)^2], \text{ for } r<1.28r_m,$$

$$= 1 \text{ for } r\geq 1.28r_m.$$

The well depth and distance parameters are ε/k = 29.80K and r_m = 3.48Å, respectively. Coefficients for the reduced potential are: $A = 7.81208 \times 10^5$; α = 13.756; C_6 = 1.28640; C_8 = 0.464948; and C_{10} = 0.227480. Whether or not the WKB approximation is reasonably accurate for a given interaction in a given velocity range has been estimated by Munn, et al [31]. The approximate calculation fails in the vicinity of classical orbiting because of tunneling and partial reflection which are not handled by the approximation. For low values of the angular momentum the centrifugal potential possesses a maximum which produces a well giving rise to two "turning points," the inner one being reached only by the tunneling process. As the angular momentum is increased, the maximum degenerates into a kink and barrier tunneling disappears, but the kink, as well as the maximum, produces partial reflection up to surprisingly high energies. Munn, et al

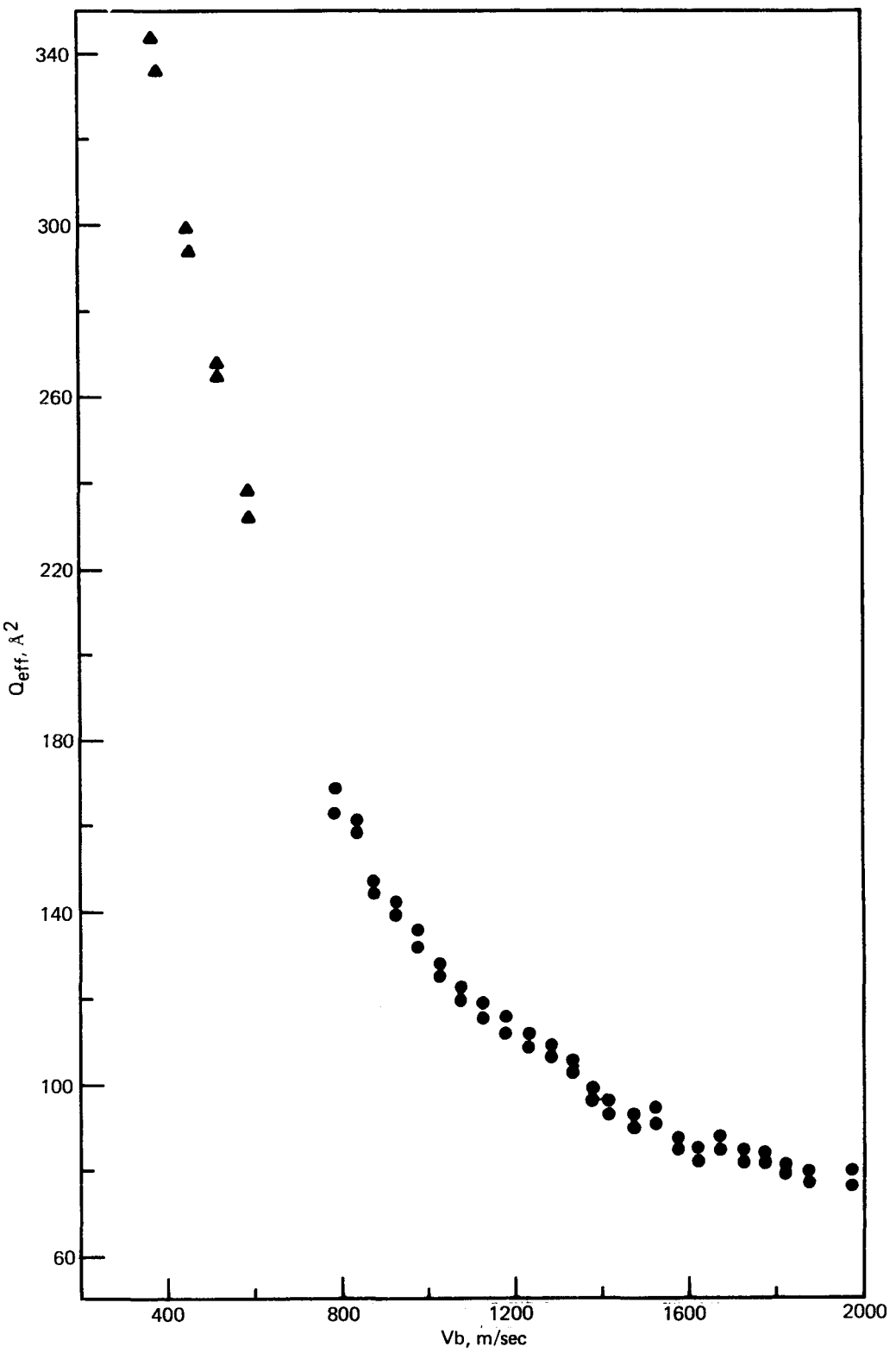

FIGURE II-6 - Effective cross section vs. beam velocity for the helium-argon system. The solid circles are helium beam with an argon target and the solid triangles are an argon beam with a helium target.

Table II-9 - EXPERIMENTAL TOTAL CROSS SECTIONS FOR THE HELIUM-ARGON SYSTEM

T_b (K)	T_t (K)	V_b (m/sec)	V_t (m/sec)	Q_{exp} (Å^2)	ΔQ (Å^2)	Q_{eff} (Å^2)	V_r (m/sec)
58.9	55	782.8	151.3	162.1	0.12	162.2	811.5
58.9	55	782.8	151.3	168.1	0.13	168.2	811.5
66.9	55	834.3	151.3	160.2	0.14	160.3	861.3
66.9	55	834.3	151.3	159.4	0.14	159.5	861.3
74.0	75	877.4	176.6	145.4	0.13	145.5	912.2
74.0	75	877.4	176.6	146.5	0.13	146.6	912.2
137.1[a]	100	377.7	645.0	330.5	13.63	344.1	947.8
137.1[a]	100	377.7	645.0	323.4	13.04	336.4	947.8
82.9	75	928.7	176.6	141.0	0.13	141.1	961.7
82.9	75	928.7	176.6	140.9	0.13	141.0	961.7
194.8[a]	100	450.2	645.0	280.7	13.55	294.2	983.3
194.8[a]	100	450.2	645.0	286.5	14.12	300.6	983.3
92.3	75	979.9	176.6	132.5	0.13	132.6	1011.
92.3	75	979.9	176.6	135.5	0.14	135.6	1011.
260.2[a]	100	520.3	645.0	252.6	14.48	267.1	1021.
260.2[a]	100	520.3	645.0	254.2	14.66	268.9	1021.
333.2[a]	100	588.8	645.0	219.0	13.87	232.9	1061.
333.2[a]	100	588.8	645.0	224.0	14.53	238.5	1061.
102.1	75	1031.	176.6	126.0	0.13	126.1	1061.
102.1	75	1031.	176.6	126.8	0.13	126.9	1061.
112.4	75	1081.	176.6	121.4	0.13	121.5	1109.
112.4	75	1081.	176.6	120.9	0.13	121.0	1109.
123.2	75	1132.	176.6	117.9	0.14	118.0	1159.
123.2	75	1132.	176.6	116.2	0.13	116.3	1159.
134.5	75	1183.	176.6	112.0	0.14	112.1	1209.
134.5	75	1183.	176.6	115.2	0.14	115.3	1209.
146.3	75	1234.	176.6	109.7	0.14	109.8	1259.
146.3	75	1234.	176.6	110.8	0.14	110.9	1259.
158.6	75	1285.	176.6	108.0	0.15	108.2	1309.
158.6	75	1285.	176.6	107.3	0.15	107.4	1309.
171.3	75	1335.	176.6	104.3	0.15	104.4	1369.
171.3	75	1335.	176.6	103.7	0.15	103.8	1369.
184.5	75	1385.	176.6	96.8	0.14	96.9	1407.
184.5	75	1385.	176.6	96.9	0.14	97.0	1407.
194.4	150	1422.	249.8	95.3	0.14	95.4	1465.
194.4	150	1422.	249.8	93.8	0.14	93.9	1465.
208.5	150	1473.	249.8	91.7	0.14	91.8	1515.
208.5	150	1473.	249.8	91.1	0.14	91.2	1515.
223.2	150	1524.	249.8	91.0	0.15	91.2	1564.
223.2	150	1524.	249.8	93.5	0.16	93.7	1564.
238.3	150	1575.	249.8	86.6	0.14	86.7	1614.
238.3	150	1575.	249.8	86.4	0.14	86.5	1614.
253.9	150	1625.	249.8	82.7	0.14	82.8	1663.
253.9	150	1625.	249.8	84.2	0.14	84.3	1663.
270.0	150	1676.	249.8	85.0	0.16	85.2	1713.
270.0	150	1676.	249.8	86.5	0.16	86.7	1713.
286.6	150	1728.	249.8	83.1	0.16	83.3	1764.
286.6	150	1728.	249.8	83.1	0.16	83.3	1764.
303.7	150	1778.	249.8	80.3	0.16	80.5	1813.
303.7	150	1778.	249.8	82.7	0.17	82.9	1813.
321.2	150	1828.	249.8	79.3	0.16	79.5	1862.
321.2	150	1828.	249.8	79.7	0.16	79.9	1862.
339.2	150	1879.	249.8	77.6	0.16	77.8	1912.
339.2	150	1879.	249.8	78.6	0.17	78.8	1912.
376.7	150	1980.	249.8	76.7	0.18	76.9	2011.
376.7	150	1980.	249.8	79.0	0.19	79.2	2011.

[a]Inverted argon-helium system.

Table II-10 - DECONVOLUTED TOTAL CROSS SECTIONS FOR THE HELIUM-ARGON SYSTEM

I_1	$I_2 \times 10^{-5}$	$I_3 \times 10^{-10}$	$\bar{V}_r$ (m/sec)	Q^I (Å^2)	Q^{II} (Å^2)
1.019	0.8267	0.6821	811.5	159.2	160.9
1.019	0.8267	0.6821	811.5	165.1	166.8
1.016	0.8754	0.7653	861.3	157.7	158.9
1.016	0.8754	0.7653	861.3	156.9	158.1
1.020	0.9307	0.8643	912.2	142.6	143.7
1.020	0.9307	0.8643	912.2	143.7	144.8
2.142[a]	2.030	2.172	947.8	160.7	160.7
2.142[a]	2.030	2.172	947.8	157.1	157.1
1.018	0.9791	0.9569	961.7	138.6	139.4
1.018	0.9791	0.9569	961.7	138.5	139.3
1.868[a]	1.836	2.032	983.3	157.5	157.5
1.868[a]	1.836	2.032	983.3	161.0	161.0
1.016	1.028	1.054	1011.	130.5	131.0
1.016	1.028	1.054	1011.	133.4	134.0
1.684[a]	1.720	1.969	1021.	158.6	158.6
1.684[a]	1.720	1.969	1021.	160.0	159.6
1.554[a]	1.649	1.954	1061.	149.8	149.8
1.554[a]	1.649	1.954	1061.	153.4	153.4
1.015	1.076	1.157	1061.	124.3	124.7
1.015	1.076	1.157	1061.	125.1	125.5
1.013	1.124	1.263	1109.	119.9	120.2
1.013	1.124	1.263	1109.	119.4	119.7
1.012	1.173	1.376	1159.	116.6	116.8
1.012	1.173	1.376	1159.	114.9	115.1
1.011	1.222	1.494	1209.	110.9	111.0
1.011	1.222	1.494	1209.	114.0	114.2
1.010	1.272	1.617	1259.	108.7	108.8
1.010	1.272	1.617	1259.	109.8	109.9
1.010	1.321	1.745	1309.	107.2	107.3
1.010	1.321	1.745	1309.	106.4	106.5
1.009	1.370	1.875	1369.	103.5	103.6
1.009	1.370	1.875	1369.	102.9	103.0
1.008	1.419	2.004	1407.	96.1	96.2
1.008	1.419	2.004	1407.	96.2	96.3
1.015	1.488	2.211	1465.	94.0	94.3
1.015	1.488	2.211	1465.	92.5	92.8
1.014	1.536	2.358	1515.	90.5	90.9
1.014	1.536	2.358	1515.	89.9	90.3
1.014	1.585	2.511	1564.	90.0	90.4
1.014	1.585	2.511	1564.	92.5	92.9
1.013	1.634	2.669	1614.	85.6	86.1
1.013	1.634	2.669	1614.	85.4	85.9
1.012	1.683	2.829	1663.	81.8	82.3
1.012	1.683	2.829	1663.	83.3	83.8
1.011	1.732	2.997	1713.	84.3	84.8
1.011	1.732	2.997	1713.	85.7	86.3
1.010	1.782	3.174	1764.	82.4	83.0
1.010	1.782	3.174	1764.	82.4	83.0
1.010	1.831	3.349	1813.	79.7	80.3
1.010	1.831	3.349	1813.	82.1	82.7
1.009	1.879	3.529	1862.	78.8	79.4
1.009	1.879	3.529	1862.	79.2	79.8
1.009	1.929	3.717	1912.	77.1	77.8
1.009	1.929	3.717	1912.	78.1	78.6
1.008	2.027	4.079	2011.	76.3	76.3
1.008	2.027	4.079	2011.	78.6	78.6

[a]Inverted argon-helium system.

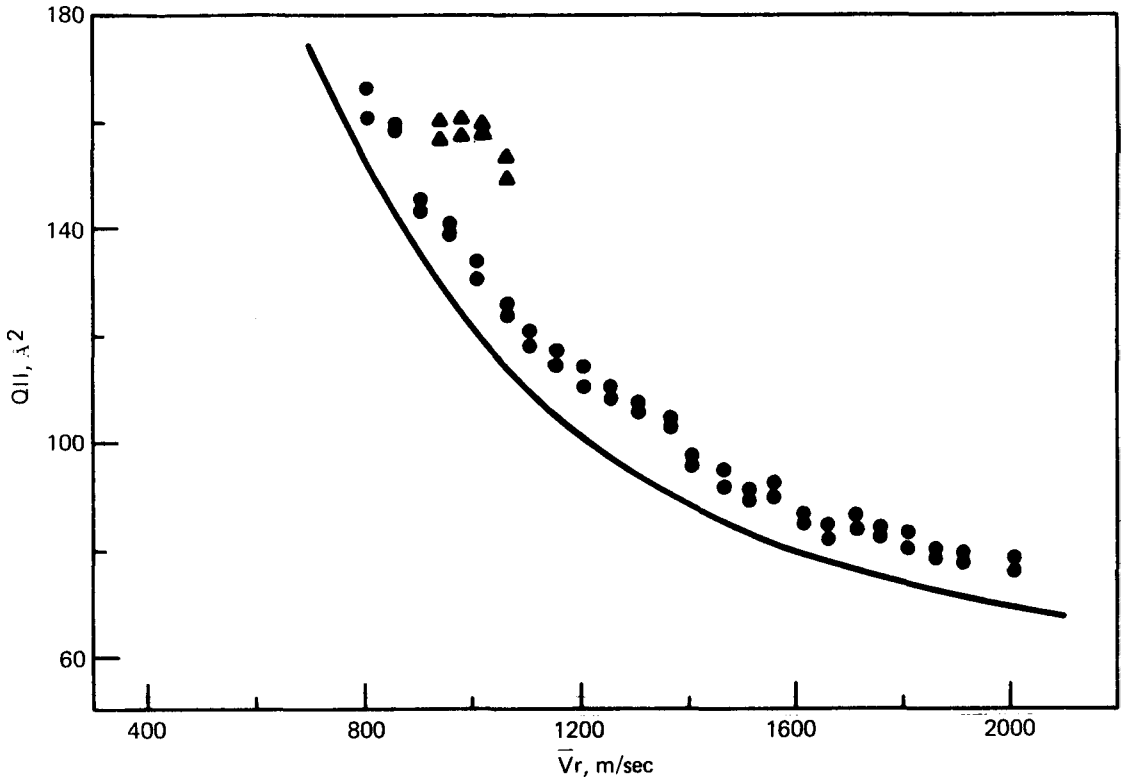

FIGURE II-7 - Deconvoluted total cross sections of the helium-argon system as a function of relative velocity. The experimental points are the same as for Figure II-6. The solid curve represents the cross section as calculated from a summation of phase shifts which were evaluated with the HFD potential using the WKB approximation.

have numerically integrated the wave equation for several values of the reduced DeBroglie wavelength, Λ^*, and give some general guidelines for applicability of the approximate calculation. In the present case the inequality

$$E/\varepsilon \gtrsim 6.2(\Lambda^*)^2 \gtrsim 5.68$$

must be satisfied. Here E is the energy of interaction and ε is the well depth. This indicates that the approximation will fail for relative velocities less than approximately 9×10^4 cm/sec for He-Ar. The approximate calculation using the HFD potential is shown by the solid curve in Figure II-7. It lies generally about 7 to 10% below the experimental data and follows the trend of the data quite closely even at low relative velocities. Noteworthy, however, is the fact that the deconvoluted inverse experiments do not agree with either the theoretical curves or the He → Ar results. Further effort will be made to reconcile this difficulty and to test the validity of the WKB calculation at low relative velocities.

III. Calculations in plutonium chemistry

Plutonium valence state distributions

G. L. Silver

It is very convenient to be able to solve plutonium valence state distribution

problems with a pocket calculator. Listed in Table III-1 is a program which calculates plutonium (or uranium and neptunium) oxidation state distributions as a function of the oxidation number of the element, the solution acidity, and the alpha coefficients for the tri-, tetra-, penta-, and hexavalent states of the element. Elsewhere, a program for determining oxidation state distributions as a function of solution redox potential has been presented [1]. Both of these programs are suitable for the HP-97 or HP-67 calculators.

To begin calculations with the program, press button "A". Then, during periods of pause, enter the following information. (Numbers in parentheses indicate typical values which have been used for plutonium in the past.) Press the Run/Stop button after each entry.

First: Enter a number which is larger than the PuO_2^{2+}/PuO_2^{+} ratio. For most problems in plutonium chemistry, 100,000 is a satisfactory choice. If the entered number is much too large, no harm is done, although the execution time of the program is lengthened. If the number is too small, the calculator will seem to calculate endlessly, or until its capacity to handle small numbers is exceeded.

Second: Enter the value of the equilibrium constant for the following reaction (6.97E-04):

$$2Pu^{4+} + 2HOH = Pu^{3+} + PuO_2^{+} + 4H^{+}. \qquad (1)$$

Third: Enter the value of the equilibrium constant for the following reaction (13.2):

$$Pu^{4+} + PuO_2^{+} = PuO_2^{2+} + Pu^{3+}. \qquad (2)$$

Fourth: Enter the number of bisection iterations desired (10 to 20).

-------LOCATION OF "B"-------

Fifth: Enter the solution equilibrium acidity in molar units.

Sixth: Enter the oxidation number of the plutonium.

Seventh-Tenth: Enter the alpha coefficients for the tri-, tetra-, penta-, and hexavalent oxidation states.

The calculator now proceeds to solve Equation (3) in Reference 2. Then the fraction of each oxidation state is presented: the trivalent state first (stored at register 3), then the tetravalent state (stored at register 4), then the pentavalent state (stored at register 5), and finally the hexavalent state (stored at register 6). (Note: a number momentarily presented, but not printed or displayed for a longer period, is the variable M, the value of the ratio of hexavalent plutonium to pentavalent plutonium. This number is momentarily displayed just before the fraction of trivalent plutonium.)

To solve another problem, press the Run/Stop button to begin the program again at location "B" (step five, which requests the molar acidity of the plutonium solution). To test the program for satisfactory operation, the quadruple point problem (for which N = 4.5) may be solved [3]. Alternatively, the equilibrium problems in Reference 2 may be solved, using the final equilibrium values of the acidity at step five.

Table III-1 - PROGRAM FOR PLUTONIUM OXIDATION STATE DISTRIBUTIONS

```
001          *Label A
              Run/Stop
              Sto E
              Sto 8
              Run/Stop
              Sto 1
              P, S Exchange
              Sto 1
              Run/Stop

010           Sto 2
              P, S Exchange
              Sto 2
              Run/Stop
              Sto 3
              P, S  Exchange
              Sto I
             *Label B
              Run/Stop
              Sto 3

020           Run/Stop
              Change Sign
              Sto 9
              Run/Stop
              Rcl 2
              Square
              Multiply
              Rcl 3
              Square
              Square

030           Multiply
              Rcl 1
              Divide
              Sto A
              Run/Stop
              Rcl 2
              Multiply
              Rcl 1
              Divide
              Rcl 3

040           Square
              Square
              Multiply
              Sto B
              Run/Stop
              Sto C
              Run/Stop
              Sto D
             *Label 1
              Rcl E

050           Sto 4
             *Label 2
              Gosub 0
              Sto 5
              X<0 ?
              Goto 3
              Rcl 4
              9
              Divide
              Sto 4

060           Goto 2
             *Label 3
              Rcl 4
              Sto 1
              9
              Multiply
              Sto 3
              Sto 4
              Gosub 0
              Sto 7

070          *Label 4
              Decrement I
              Goto 5
              Goto 9
             *Label 5
              Rcl 1
              Rcl 3
              Add
              2
              Divide

080           Sto 4
              Gosub 0
              Sto 6
              Rcl 5
              Multiply
              X<0 ?
              Goto 6
              Goto 7
             *Label 6
              Rcl 4

090           Sto 3
              Goto 4
             *Label 7
              Rcl 6
              Rcl 7
              Multiply
              X<0 ?
              Goto 8
              Goto 9
             *Label 8
```

```
100     Rcl 4
        Sto 1
        Goto 4
       *Label 0
        Rcl 4
        Square
        Rcl 4
        Multiply
        Rcl D
        Multiply

110     Rcl 9
        6
        Add
        Multiply
        Rcl 4
        Square
        Rcl C
        Multiply
        Rcl 9
        5

120     Add
        Multiply
        Add
        Rcl B
        Rcl 4
        Multiply
        Rcl 9
        4
        Add
        Multiply

130     Add
        Rcl A
        Rcl 9
        3
        Add
        Multiply
        Add
        Return
       *Label 9
        Rcl 4

140     Sto 7
        Pause
        Rcl A
        Rcl 7
        Square
        Divide
        Sto 3
        Sto 0
        Rcl B
        Rcl 7

150     Divide
        Sto 4
        Sto + 0
        Rcl C
        Sto + 0
        Rcl D
        Rcl 7
        Multiply
        Sto 6
        Sto + 0

160     Rcl 3
        Rcl 0
        Divide
        Sto 3
        Print X
        Rcl 4
        Rcl 0
        Divide
        Print X
        Sto 4

170     Rcl C
        Rcl 0
        Divide
        Print X
        Sto 5
        Rcl 6
        Rcl 0
        Divide
        Sto 6
        Print X

180     Run/Stop
        Clear Registers
        P, S Exchange
        Rcl 1
        Sto A
        Rcl 2
        Sto B
        Rcl 3
        Sto I
        Rcl 8

190     Sto E
        P, S Exchange
        Rcl A
        Sto 1
        Rcl B
        Sto 2
        Goto B
```

The number of bisection operations is an option available to the user. At least ten of these iterations are recommended. More iterations lengthen the computation time, but increase the accuracy of the answers. With twenty iterations, a typical problem in plutonium chemistry might require about two minutes for execution.

Improved algorithm for three variable minimization problems

G. L. Silver

Recently, two and three variable optimization routines were presented [4]. These routines are useful for the study of chemical equilibrium by the method of proportional equations [5]. Table III-2 presents a three variable optimization routine that is more convenient to use than the previously presented routine. The manner of entering data is the same as the previously described routine, but a different set of registers is used. Enter the coordinates of the initial points as follows:

POINT	REGISTERS	FUNCTION VALUE REGISTER
X1,Y1,Z1	7,11,15; 10,14,18	3
X2,Y2,Z2	8,12,16; 10,14,18	4
X3,Y3,Z3	9,13,17; 10,14,18	5
X4,Y4,Z4	10,14,18	6

The function is stored at Label Zero. (Table III-2 contains the function $X^2 + Y^2 + Z^2$ at Label Zero to illustrate recall of trial values of the points.) Registers 0, 1, 2, A, B, C, D, E, 19 are available for storage of miscellaneous data. The X, Y, and Z coordinates of the best point can be recalled from registers 7, 11, and 15, respectively.

Environmental plutonium

G. L. Silver

In a short paper on the stability of pentavalent plutonium [6], Silver showed that the concentration of plutonium(V) in an aqueous solution could be written as:

$$[PuO_2^+] = [Pu]_t/F \qquad (1)$$

where $[Pu]_t$ is the total plutonium concentration, and "F" contains terms relating to the acidity and the potential (vs. N.H.E.) of the solution. The concentration of tetravalent plutonium may be taken as [7]:

$$[Pu^{4+}] = \frac{K_2[H^+]^4[PuO_2^+]}{K_1 M} \qquad (2)$$

The concentration of tetravalent plutonium may therefore be expressed in terms of the total plutonium concentration:

$$[Pu^{4+}] = \frac{K_2[H^+]^4[Pu]_t}{K_1 MF} \qquad (3)$$

in which M is the ratio $[PuO_2^{2+}]/[PuO_2^+]$ and is related to the solution oxidation-reduction potential by the Nernst equation. Since both sides are equal to unity, the following equation may be formulated:

$$\frac{\text{total concentration of Pu(IV)}}{\text{total concentration of Pu(IV)}} = \frac{\text{total concentration of Pu(V)}}{\text{total concentration of Pu(V)}} \qquad (4)$$

and is useful because of the variety of ways of expressing total concentrations. Thus, if the solubility product of tetravalent plutonium hydroxide is 10^{-55}, then $[Pu^{4+}] = 10[H^+]^4$. Hence,

Table II-2 - THREE VARIABLE MINIMIZATION ROUTINE

```
001   *Label A
       Clear Flag 2
       Clear Flag 3
       Gosub B
       Gosub B
      *Label C
       Clear Flag 0
       Gosub B
       Rcl 3
010    Pause
      *Label E
       1
       0
       Gosub 3
       Gosub 3
       Gosub 3
       Gosub 0
       Flag 2?
       Sto 6
020    Flag 3?
       Goto C
       Rcl 4
       X ≤ Y?
       Goto D
       Exchange X & Y
       Sto 6
       Goto C
      *Label D
       Set Flag 0
030    Set Flag 2
       Set Flag 3
       Goto E
      *Label B
       6
       Sto I
       Gosub 1
       5
       Sto I
       Gosub 1
040    4
       Sto I
       Gosub 1
       Return
      *Label 1
       Rcl (i)
       Decrement I
       Rcl (i)
       X ≤ Y?
       Return
050    Exchange X & Y
       Sto (i)
       Increment I
       Stack Roll Down
       Sto (i)
       Gosub 2
       Gosub 2
       Gosub 2
       Return
      *Label 2
060    Rcl I
       4
       Add
       Sto I
       Rcl (i)
       Decrement I
       Rcl (i)
       Exchange X & Y
       Sto (i)
       Increment I
070    Stack Roll Down
       Sto (i)
       Return
      *Label 3
       Sto I
       Rcl (i)
       Decrement I
       Rcl (i)
       Decrement I
       Rcl (i)
080    Add
       Decrement I
       Rcl (i)
       Add
       3
       Divide
       Subtract
       Last X
       Exchange X & Y
       Decimal
090    4
       Flag 0?
       Goto 4
       Clear X
       1
       Decimal
       2
       5
      *Label 4
       Multiply
100    Subtract
       Increment I
       Increment I
       Increment I
       Sto (i)
       Rcl I
       4
       Add
       Return
      *Label 0
110    P, S Exchange
       Rcl 0
       Square
       Rcl 4
       Square
       Add
       Rcl 8
       Square
       Add
       P, S Exchange
120    Return
```

$$\frac{\frac{K_2[H^+]^4[Pu]_t}{K_1MF}}{10[H^+]^4} = \frac{[Pu]_t/F}{\text{total concentration of Pu(V)}} \qquad (5)$$

It follows that total concentration of Pu(V) is:

$$[PuO_2^+]_t = \frac{10\ K_1M}{K_2} \qquad (6)$$

since the term $[Pu]_t$ disappears by cancellation. (The number "10" in this equation derives from approximating the solubility product of $Pu(OH)_4$ as 10^{-55}.) Equation (6) states that the total concentration of pentavalent plutonium in equilibrium with $Pu(OH)_4$ depends on the numerical values of the solubility product of $Pu(OH)_4$, as well as the values of K_1, K_2, and M.

That the total concentration of pentavalent plutonium in equilibrium with plutonium(IV) hydroxide does not depend on the solution's acidity may seem surprising at first, but it should be recalled that, while the total soluble plutonium increases rapidly with acidity:

$$Pu(OH)_4 + 4H^+ \rightarrow \text{products [including Pu(V)]} \qquad (7)$$

the concentration of pentavalent plutonium diminishes rapidly with increasing acidity:

$$2PuO_2^+ + 4H^+ \rightarrow \text{products} \qquad (8)$$

so that the simultaneous effect of Equations (7) and (8) is to keep $[PuO_2^+]_t$ constant. This constancy of the concentration of $[PuO_2^+]_t$ may be checked with the oxidation state distribution program described elsewhere [8]. Of course, Equation (6) does not consider complexation effects. It seems to be commonly held, however, that plutonium(V) is not complexed in environmental systems. If this is the case, Equation (6) may be very useful for estimating Pu(V) concentrations in the environment, provided that it is in equilibrium with tetravalent plutonium hydroxide. [It is curious that Equation (6), or a similar equation, has not been pointed out before, and that no attempt has ever been made to use it.] If pentavalent plutonium is complexed in environmental systems, then Equation (6) is inapplicable, but may be made applicable by multiplying the right hand side of the equation by the Pu(V) alpha coefficient, denoted (AY).

How are plutonium alpha coefficients to be measured? This is a problem which has never received adequate attention. Consider, however, a cation exchange resin partially loaded with trivalent neodymium as a substitute for trivalent plutonium. If the resin were equilibrated with distilled water containing the same mineral composition (and therefore ionic strength) as a sample of natural water, a certain equilibrium concentration of Nd^{3+} ions would soon be established. If another portion of the same resin were equilibrated with natural water, the same Nd^{3+} concentration would be established, plus some soluble neodymium complexed by the naturally occurring organic materials in the environmental water. The total soluble neodymium in the first case is $[Nd^{3+}]$, whereas in the second case it is $[NdL] + [Nd^{3+}]$, where [NdL] symbolizes all complexed neodymium. The ratio of these two neodymium concentrations, $([Nd^{3+}] + [NdL])/[Nd^{3+}]$, is an approximation to the alpha coefficient for neodymium in the natural water. Since Nd^{3+}

and Pu^{3+} are similar in many ways, this approximation may suffice as an approximation of the Pu(III) alpha coefficient in natural water. Since alpha coefficients in environmental systems may display a dependence on metal ion concentration, the experiment should probably be repeated with resins of varying affinities for neodymium.

Effect of temperature upon pentavalent plutonium disproportionation

G. L. Silver

Several years ago, a paper purporting to describe the pentavalent plutonium disproportionation stoichiometry as a function of temperature was published [9]. In deriving the stoichiometry coefficients, the paper arbitrarily let the stoichiometry coefficient for trivalent plutonium be unity. What is the justification for this assignment?

The disproportionation of plutonium(V) consumes hydrogen ions and generates water molecules. But, if for the purpose of simplifying calculations, the acidity of the solution is supposed constant (a common assumption in chemistry for the purpose of problem solving), then the rearrangement of plutonium oxidation states is an isomolecular reaction; the numbers of reactant species [Pu(V)] which disappear are equal to the numbers of product species which appear. In other words, if

$$A[Pu(V)] = B[Pu(III)] + C[Pu(IV)] + D[Pu(VI)] \quad (1)$$

then A = B + C + D, and if (B + C + D) particles of product appear, then (A) particles of reactant have disappeared. In such cases, the basis for computing the relationships among the species can be arbitrarily assigned, and it is most helpful to remember this. The situation is perhaps illuminated by an analogy.

A large meadow is divided into four pastures. Shepherds A, B, C, and D each herd their sheep into a separate pasture, and then meet for shepherd talk. Shepherd C says, "I have more sheep now than ever before." Shepherd A responds, "That may be, but I have three times as many sheep as are in your little flock." Shepherd B boasts that he has five times as many sheep as Shepherd C, and Shepherd D exclaims that he has seven times as many sheep as Shepherd C.

What percentage of all the sheep has Shepherd C? If Shepherd C has Y number of sheep, the other shepherds must have 3Y, 5Y, and 7Y sheep, respectively, so that the fraction of the total sheep herded by Shepherd C is $Y/(Y + 3Y + 5Y + 7Y) = 1/16$. It does not matter how many sheep Shepherd C actually possesses, his fraction is always 1/16 of the total sheep in the meadow. The problem can be solved by letting Y = 1, or any other number.

As it is with sheep, so it is with plutonium, for the Nernst equation (used with reported oxidation-reduction potentials) can be used as a substitute for shepherd talk, providing ratios of oxidation states. Valence state distribution problems may then be solved as well by letting Pu(III) = 1 as any other number. Similarly, some other shepherd's sheep (oxidation state) could also be assigned as unity for the purpose of evaluating

distributions of sheep (or distributions of oxidation states). Suppose the shepherds herd their sheep as one large flock. If they later divide the large flock by right of ownership, each of the four shepherds may talk of the size of his own flock as before. The act of splitting the large flock into separate groups is analogous to the reaction of disproportionation. It is only necessary to hear the shepherds talk to assign the relative number of sheep to each flock; likewise, it is only necessary to use the Nernst equation to obtain a relationship among products of disproportionation.

Now, suppose that only three shepherds talk while the fourth shepherd mends fences. Then it will be possible to determine the relative sizes of only three of the flocks (as outlined above), while the size of the fourth flock remains unknown. For these three flocks, an equation may be written:

$$(A+B+C) \text{ sheep} = (A) \text{ sheep} + (B) \text{ sheep} + (C) \text{ sheep} \qquad (2)$$

and the relative magnitudes of A, B, and C, which derive from splitting part of the original flock may be assessed by information gleaned from the shepherds' talk. In the case of plutonium (but not of sheep) the splitting pattern depends on the temperature, and this pattern may be obtained with the aid of the Nernst equation [9]. To ascertain the size of the fourth flock, more information is necessary. Here the analogy breaks down, for the fourth piece of information in plutonium chemistry may be taken as an equilibrium constant, something which has no parallel among sheep [10].

The analogy with sheep is helpful for pointing out other interesting facets of the disproportionation reaction.

1. Each oxidation state may be expressed in terms of Pu(III) as well as any other oxidation state. Thus,

$$[Pu(III)] = [Pu(III)] \qquad (2)$$

(which says that the number of sheep possessed by Shepherd A is equal to the number of sheep possessed by Shepherd A);

$$[Pu(IV)] = \frac{M}{K_2} [Pu(III)] \qquad (3)$$

(which says that the number of sheep possessed by Shepherd B is equal to a constant times the number of sheep possessed by Shepherd A). Likewise,

$$[Pu(V)] = \frac{K_1 M^2}{K_2^2 H^4} [Pu(III)] \qquad (4)$$

$$[Pu(VI)] = \frac{K_1 M^3}{K_2^2 H^4} [Pu(III)] \qquad (5)$$

in which the symbols K_1, K_2, H, and M have their usual meanings [11]. But in no case does computation of the fractions, proportions, or relative magnitudes of each oxidation state depend on the value assigned to [Pu(III)]. Therefore, to make the problem simpler, let [Pu(III)] = 1.

2. Recognizing that the frame of reference for computations can be any oxidation state whatsoever is most convenient when solving problems by the method of proportional equations [12].

The conclusions reached in Reference [9], which can be understood in terms of the sheep analogy, can be checked by other

techniques which do not depend on analogies [13]. Moreover, the complete valence state distribution for pentavalent plutonium (N=5.00) in 1M acid may be computed using the methods described in Reference 14 or Reference 15 with the aid of the formal potentials given in Cleveland's book [16]. From the oxidation state distribution, the stoichiometry of disproportionation at 25°C may be determined [17]. The stoichiometry coefficients so derived are similar (but not identical) to the stoichiometry coefficients at 25°C given in Reference 9. (The reason for the inexact correspondence is the fact that coefficients of disproportionation derived, as in Reference 9, depend on the values of only two formal potentials, and are therefore subject to error only so far as the two formal potentials may be subject to error. But the computation of a complete oxidation state distribution requires more than two formal potentials, and stoichiometry coefficients computed from a complete oxidation state distribution are therefore more liable to error.)

The justification for the apparently arbitrary Pu(III) = 1 assignment may also be understood in a purely algebraic way. Divide all plutonium concentrations in Reference 9 which appear as arguments of logarithms by [Pu(III)]. Similarly, divide each side of the charge conservation statement for N = 5.00 by [Pu(III)]:

$$\frac{[Pu(VI)]}{[Pu(III)]} = \frac{[Pu(IV)]}{[Pu(III)]} + 2\,\frac{[Pu(III)]}{[Pu(III)]} \qquad (6)$$

Then the term [Pu(IV)] in the equation

$$3 \log [Pu(IV)] - \log [Pu(IV) + 2] = \text{constant} \qquad (7)$$

(which is Equation (3) in Reference 9) becomes the ratio [Pu(IV)]/[Pu(III)]. The value of this ratio is found to be about 24. By Equation (6), therefore, the ratio [Pu(VI)]/[Pu(III)] is about 26, since [Pu(III)]/[Pu(III)] = 1. Now, if the disproportionation of pentavalent plutonium generates one part of trivalent plutonium, it must therefore generate about 24 parts of tetravalent plutonium, and also about 26 parts of hexavalent plutonium. The quantity of pentavalent plutonium which generated this distribution was therefore about (1+24+26) = 51 times the amount of trivalent plutonium. The stoichiometry of disproportionation is therefore:

$$51\,\frac{Pu(V)}{Pu(III)} = \frac{Pu(III)}{Pu(III)} + 24\,\frac{Pu(IV)}{Pu(III)} + 26\,\frac{Pu(VI)}{Pu(III)} \qquad (8)$$

from which Pu(III), whatever its value, disappears by cancellation [18]:

$$51[Pu(V)] = [Pu(III)] + 24[Pu(IV)] + 26[Pu(VI)] \qquad (9)$$

It is an easy task to balance Equation (9) with protons and water molecules.

This ratio technique has been described in detail in another paper where it has been applied to the chemistries of uranium and neptunium [19].

References

I. Low temperature research

1. NBS Monograph 126, Platinum Resistance Thermometry, April 1973.

2. Rosemont Engineering type 146-L Platinum Thermometer #2788, Calibration August 31, 1966.

3. G. T. Furukawa, Metrologia 8, 11 (1972).

4. E. R. Grilly, Cryogenics, 2, 226 (1962).

5. E. R. Grilly, J. Am. Chem. Soc., 73, 843 (1951).

6. A. Bellamans and H. Bablyantz, Mol. Physics, 2, 169 (1959).

7. W. K. Meckstroth and David White, J. Chem. Phys., 34, 3723 (1971).

8. M. W. Lee, S. Fuks, J. Begeleisen, J. Chem. Phys., 53, 4066 (1970).

9. L. Wolniewicz, J. Chem. Phys., 45, 515, (1966).

10. P. C. Souers, Cryogenic Hydrogen Data Pertinent to Magnetic Fusion Energy, UCRL-52628 (March 15, 1979).

11. J. M. Farrar and Y. T. Lee, J. Chem. Phys., 57, 5429 (1972).

12. G. T. McConville, J. Chem. Phys., (to be published 2/15/81).

II. Separation research

1. Mound Facility Activities in Chemical and Physical Research: January-June 1980, MLM-2756 (Aug. 29, 1980), p. 17.

2. Mound Facility Activities in Chemical and Physical Research: July-December 1979, MLM-2727 (June 18, 1980), p. 21.

3. W. M. Rutherford, J. Chem. Phys., 59, 6061 (1973).

4. Mound Facility Activities in Chemical and Physical Research: January-June 1977, MLM-2450 (Oct. 4, 1977), p. 40.

5. Mound Facility Activities in Chemical and Physical Research: July-December 1979, MLM-2727 (June 18, 1980), p. 28.

6. Mound Facility Activities in Chemical and Physical Research: January-June 1979, MLM-2654 (Oct. 29, 1979), p. 18.

7. H. Korsching, Z. Naturforsch, 7b, 187 (1951).

8. W. M. Rutherford, Separation and Purification Methods, 4, 305 (1975).

9. P. H. Abelson, N. Rosen and J. I. Hoover, Liquid Thermal Diffusion, USAEC Report TID-5229, August 1958.

10. H. Korsching and K. Wirtz, Naturwiss., 27, 367 (1939).

11. G. Panson, Dissertation, Columbia University, N. Y., 1953.

12. P. Varga-Manyi, Acta Biochem. and Biophys. Acad. Sci. Hung., 1, 197 (1966).

13. G. D. Rabinovich, V. I. Shinkevich and K. K. Azroyan, Inzh. Fiz. Zh., 37, 76 (1979).

14. Mound Facility Activities in Chemical and Physical Research: January-June 1980, MLM-2756 (August 29, 1980), p.20.

15. Mound Facility Activities in Chemical and Physical Research: January-June 1980, MLM-2756 (August 29, 1980), p. 47; also July-December 1979, MLM-2727 (June 18, 1980), p. 42.

16. K. G. Heuman and Hans-Peter Schiefer, "Calcium Isotope Separation on an Exchange Resin Having Cryptand Anchor Groups," Angew. Chem. Int. Ed., 19, (1980), pp. 406-407.

17. Mound Facility Activities in Chemical and Physical Research: January-June 1980, MLM-2756 (August 29, 1980), pp. 35-47.

18. R. E. Ellefson, "Factors Involved in Quantitative Gas Analysis by Mass Spectrometry," presented at the 22nd Rocky Mountain Conference, Rocky Mountain Society for Applied Spectroscopy and R. M. Chromatography Group, Denver, Colorado, 11-14 August 1980, MLM-2794(OP).

19. W. Hogervorst, Physica, 51, 59 (1971).

20. P. E. Suetin, B. A. Kelinen, and A. E. Loiko, Sov. Phys. Tech. Phys., 15, 1349 (1971).

21. B. A. Kalinen and P. E. Suetin, Heat Transfer - Sov. Res., 7, 146 (1975).

22. J. C. Liner and S. Weissman, J. Chem. Phys., 56, 2288 (1972).

23. T. R. Marrero and E. A. Mason, J. Phys. Chem. Ref. Data, 1, 1 (1972).

24. P. S. Arora, H. L. Robjohns and P. J. Dunlop, Physica, 95A, 561 (1979).

25. V. P. S. Nain and R. A. Aziz, Molec. Phys., 33, 303 (1977).

26. R. A. Aziz, private communication.

27. Mound Facility Activities in Chemical and Physical Research: January-June 1980, MLM-2756 (August 29, 1980), pp. 25-35.

28. W. L. Taylor, R. W. York and P. T. Pickett, "Velocity Dependence of Low-Energy Neon-Argon Total Cross Sections," to be published in the proceedings of the Twelfth International Symposium of Rarefied Gas Dynamics, Charlottesville, Virginia, July 1980.

29. Mound Laboratory Activities for the Division of Physical Research: January June 1976, MLM-2354 (September 30, 1976), pp. 40-48.

30. R. A. Aziz, P. W. Riley, J. Buck, G. Maneki, J. Schleusener, G. Scoles and J. Valbusa, J. Chem. Phys., 71, 2637 (1979).

31. R. J. Munn, E. A. Mason and F. J. Smith, J. Chem. Phys., 41, 3978 (1964).

III. Calculations in plutonium chemistry

1. Mound Facility Activities in Chemical and Physical Research: July-December 1979, MLM-2727 (June 18, 1980), p. 48.

2. G. L. Silver, Radiochimica Acta, 21, 54 (1974).

3. G. L. Silver, J. Inorg. Nucl. Chem., 34, 1857 (1972).

4. Mound Facility Activities in Chemical and Physical Research: July-December 1979, MLM-2727 (June 18, 1980), p. 48.

5. G. L. Silver, Radiochem. Radioanal. Letters, 27(4), 243 (1976).

6. G. L. Silver, J. Inorg. Nucl. Chem., 35, 1369 (1973).

7. G. L. Silver, Radiochimica Acta, 21, 54 (1974).

8. Mound Facility Activities in Chemical and Physical Research: July-December 1979, MLM-2727 (June 18, 1980), p. 47.

9. G. L. Silver, J. Inorg. Nucl. Chem., 34, 1857 (1972).

10. G. L. Silver, Aqueous Plutonium Chemistry, Some Minor Problems, MLM-1871 (May 26, 1972), 68 pp.

11. G. L. Silver, Radiochimica Acta, 21, 54 (1974).

12. G. L. Silver, Optimization Algorithm, MLM-2638 (August 24, 1979), 11 pp.

13. G. L. Silver, Minor Problems in Aqueous Plutonium Chemistry, MLM-2075 (October 1, 1973), 55 pp.

14. G. L. Silver, J. Radioanal. Chem., 23, 195 (1974).

15. G. L. Silver, Radiochimica Acta, 21, 54 (1974).

16. J. M. Cleveland, The Chemistry of Plutonium, Gordon and Breach Science Publishers, New York, 1970, p. 20.

17. G. L. Silver, J. Inorg. Nucl. Chem., 33, 577 (1971) and 33, 4000 (1971).

18. G. L. Silver, J. Radioanal. Chem., 23, 195 (1974).

19. G. L. Silver, Radiochem. Radioanal. Letters, 10(5), 291 (1972).

Distribution

EXTERNAL

TID-4500, UC-4 and UC-22 (194)

Technical Report Library, Monsanto, St. Louis

H. N Hill, DOE/Dayton Area Office
R. B. Craner, Sandia Laboratories Albuquerque
D. Emin, Sandia Laboratories Albuquerque
B. Morosin, Sandia Laboratories Albuquerque
P. M. Richards, Sandia Laboratories Albuquerque
A. C. Switendick, Sandia Laboratories Albuquerque
E. L. Venturini, Sandia Laboratories Albuquerque
R. K. Flitcraft, Monsanto Research Corporation
W. J. Haubach, DOE/Division of Basic Energy Sciences
N. Haberman, DOE/Division of Advanced Nuclear Systems and Projects
J. R. Blair, DOE/Division of Biomedical and Environmental Research
F. D. Stevenson, DOE/Division of Basic Energy Sciences
C. P. Sutter/R. N. Diebel, Atlantic Richfield
D. White, University of Pennsylvania
J. N. Maddox, DOE/Office of Health and Environmental Research

INTERNAL

W. R. Amos
D. Cain
W. T. Cave
C. W. Huntington
B. E. Jepson
J. R. McClain
G. T. McConville
E. D. Michaels
G. C. Shockey
G. L. Silver
W. M. Rutherford
W. L. Taylor
R. E. Vallee
K. D. Westrick
W. R. Wilkes
L. J. Wittenberg
R. W. York
Document Control
Library (15)
Publications

Published by Information Services:
Stephen L. Nowka, Editor